

Bipartite Mixed Membership Distribution-Free Model. A novel model for community detection in overlapping bipartite weighted networks

Huan Qing

QINGHUAN@CUMT.EDU.CN;QINGHUAN07131995@163.COM

School of Mathematics

China University of Mining and Technology

Xuzhou, 221116, P.R. China

Abstract

Modeling and estimating mixed memberships for un-directed un-weighted networks in which nodes can belong to multiple communities has been well studied in recent years. However, for a more general case, the bipartite weighted networks in which nodes can belong to multiple communities, row nodes can be different from column nodes, and all elements of adjacency matrices can be any finite real values, to our knowledge, there is no model for such bipartite weighted networks. To close this gap, this paper introduces a novel model, the Bipartite Mixed Membership Distribution-Free (BiMMDF) model. As a special case, bipartite signed networks with mixed memberships can also be generated from BiMMDF. Our model enjoys its advantage by allowing all elements of an adjacency matrix to be generated from any distribution as long as the expectation adjacency matrix has a block structure related to node memberships under BiMMDF. The proposed model can be viewed as an extension of many previous models, including the popular mixed membership stochastic blockmodels. An efficient algorithm with a theoretical guarantee of consistent estimation is applied to fit BiMMDF. In particular, for a standard bipartite weighted network with two row (and column) communities, to make the algorithm's error rates small with high probability, separation conditions are obtained when adjacency matrices are generated from different distributions under BiMMDF. The behavior differences of different distributions on separation conditions are verified by extensive synthetic bipartite weighted networks generated under BiMMDF. Experiments on real-world directed weighted networks illustrate the advantage of the algorithm in studying highly mixed nodes and asymmetry between row and column communities.

Keywords: Community detection, complex networks, distribution-free model, overlapping bipartite weighted networks.

1. Introduction

Complex networks are ubiquitous in our daily life. For example, food networks Dunne et al. (2002), social networks Palla et al. (2007); Pizzuti (2008); Bedi and Sharma (2016), coauthorship and citation networks Newman (2004a); Ji and Jin (2016); Ji et al. (2022), and biological networks Barabasi and Oltvai (2004); Guimera and Nunes Amaral (2005); Notebaart et al. (2006); Rubinov and Sporns (2010); Su et al. (2010). Wonderful reviews of complex networks and technique literature have been provided by Newman (2003); Goldenberg et al. (2010).

Community detection is one of the most powerful tools in learning latent structure of complex networks. The main goal of community detection is to find group of nodes. Usually, it is assumed that nodes have more links within communities than across communities for assortative networks, and nodes have more links across communities than within communities for dis-assortative networks Newman (2002). For networks in which some nodes have weak intra-connection, some nodes have strong intra-connection, some nodes have weak inter-connection, and some nodes have strong inter-connection, a null statistical model is used to model such networks. Generally speaking, for static networks considered in this article, they mainly consist of four cases: un-directed un-weighted networks, directed un-weighted networks, un-directed weighted networks, and directed weighted

networks. We will first briefly introduce representative statistical models for these four cases and then introduce our main contributions.

For community detection of un-directed un-weighted networks, it has been widely studied for decades Fortunato (2010); Papadopoulos et al. (2012); Fortunato and Hric (2016); Javed et al. (2018); Jin et al. (2021); Fortunato and Newman (2022). The Stochastic Blockmodel (SBM) Holland et al. (1983) is one of the most popular generative models to describe community structure for such networks. SBM assumes that the probability of a link between two nodes is determined by node communities. Benefiting from the block structure, SBM can describe community structure for networks more than assortative and dis-assortative networks. From now on, we mainly focus on SBM-based models in previous literature, where SBM-based models mean that models are extensions of SBM. Though SBM is mathematically simple and easy to analyze, it always performs poorly on real-world networks since SBM assumes that nodes in the same community have the same expected degree. The Degree-Corrected Stochastic Blockmodels (DCSBM) Karrer and Newman (2011) was proposed to address this limitation by considering the node heterogeneity parameters. To detect communities of networks generated from SBM and DCSBM, substantial works have been proposed in recent years, including algorithms designed by maximizing the likelihood Karrer and Newman (2011); Bickel and Chen (2009); Zhao et al. (2012), methods for optimization via low-rank approximation Le et al. (2016), methods via convexified modularity maximization Chen et al. (2018), and spectral clustering algorithms Rohe et al. (2011); Qin and Rohe (2013); Jin (2015); Lei and Rinaldo (2015); Joseph and Yu (2016). For a comprehensive review of recent developments about SBM, see Abbe (2017). One main limitation of SBM and DCSBM is, they assume that each node only belongs to a sole community and does not allow overlapping scenarios. The classical Mixed Membership Stochastic Blockmodels (MMSB) Airoldi et al. (2008) was proposed as an extension of SBM by allowing nodes to belong to multiple communities. The Degree-Corrected Mixed Membership (DCMM) model introduced in Jin et al. (2017) can be seen as an extension of MMSB by considering node heterogeneity parameter, and it can also be seen as an extension of DCSBM from non-overlapping networks to overlapping networks. The Overlapping Continuous Community Assignment Model (OCCAM) Zhang et al. (2020) equals DCMM, the Stochastic Blockmodel with Overlaps (SBMO) Kaufmann et al. (2018) is a special case of DCMM, and the Overlapping Stochastic Block Models (OSBM) Latouche et al. (2011) is interesting because it assumes that the probability of generating an edge between two nodes depends on a product of exponential function and logistic sigmoid function. To estimate mixed memberships of networks generated from MMSB and DCMM, some methods are proposed, including MCMC Airoldi et al. (2008), variational approximation method Gopalan and Blei (2013), nonnegative matrix factorization inference methods Ball et al. (2011); Psorakis et al. (2011); Wang et al. (2011, 2016); Mao et al. (2017), tensor-based method Anandkumar et al. (2013), and spectral methods Jin et al. (2017); Mao et al. (2018); Zhang et al. (2020); Mao et al. (2020). For a general review on overlapping community detection, see Xie et al. (2013).

For community detection of directed un-weighted networks, it has been widely studied more than ten years Leicht and Newman (2008); Malliaros and Vazirgiannis (2013). Some interesting and meaningful SBM-based statistical models have been proposed for such networks in recent years. Rohe et al. (2016) proposed Stochastic co-Blockmodel (ScBM) and Degree-Corrected Stochastic co-Blockmodel (DCScBM) to model directed un-weighted networks in which nodes have no mixed memberships. ScBM and DCScBM can be seen as direct extensions of SBM and DCSBM from un-directed un-weighted networks to directed un-weighted networks, respectively. Especially, both ScBM and DCScBM allow row nodes to be different from column nodes, so they can model bipartite un-weighted networks. Spectral algorithms with theoretical guarantees on consistent estimation and one algorithm designed by co-clustering via NMF have been designed to estimate groups of nodes under ScBM and DCScBM, see algorithms proposed in Rohe et al. (2016); Zhou and A.Amini (2019); Wang et al. (2020). Similar to SBM, ScBM also can not model mixed membership networks. The Directed Mixed Membership Stochastic Blockmodels (DiMMSB) Qing and Wang (2021) was proposed to address this limitation by allowing both row and column nodes to belong to multiple

communities in a bipartite un-weighted network. DiMMSB can be seen as a direct extension of MMSB from un-directed un-weighted networks to directed un-weighted networks, and it can also be seen as an extension of ScBM from non-overlapping directed un-weighted networks to overlapping directed un-weighted networks. To estimate memberships under DiMMSB, Qing and Wang (2021) designed a spectral algorithm with a theoretical guarantee of estimation consistency.

For community detection of un-directed weighted networks, it has been an interesting topic in recent years. Edge weights are important and meaningful in a network since they can improve community detection Newman (2004b); Barrat et al. (2004). Newman (2004b) studied a weighted network in which edge weights are nonnegative integers. To study a weighted network in which edge weights are more than nonnegative integers, many models extend SBM from un-directed un-weighted networks to un-directed weighted networks. Some Weighted Stochastic Blockmodels (WSBM) are developed recent years Aicher et al. (2015); Ahn et al. (2018); Palowitch et al. (2017); Xu et al. (2020); Ng and Murphy (2021). However, these WSBM always limit the block matrix to having nonnegative entries or require edge weights to follow certain distributions, and it is a challenge to design spectral algorithms to fit these models. The Distribution-Free models (DFM)Qing (2021) was proposed to overcome these limitations. DFM allows the adjacency matrix to come from any distribution as long as the expectation adjacency matrix has a block structure reflecting community structure. Another advantage of DFM is, similar to SBM, spectral algorithms are allowed to fit DFM. The distribution-free idea introduced in Qing (2021) is significant and it is closely related to the model developed in this paper. DCDFM Qing (2022b) extends DFM by considering node heterogeneity parameters and it can also be seen as a direct extension of DCSBM from un-directed un-weighted networks to un-directed weighted networks. However, all these WSBM, DFM and DCDFM have one main limitation, each node only belongs to one community under these models. To model overlapping un-directed weighted networks, the Weighted version of the MMSB (WMMSB) model Dulac et al. (2020) was proposed as an extension of MMSB by allowing edge weights to come from Poisson distribution. The Mixed Membership Distribution-Free (MMDF) model takes the advantage of distribution-free idea and extends MMSB by allowing edge weights to come from any distribution. Compared to WMMSB, MMDF is more applicable since it has no constraint on distribution.

For community detection of directed weighted networks, this problem is more general than the above three cases since un-directed un-weighted networks, directed un-weighted networks and un-directed weighted networks can be seen as sub-networks of directed weighted networks. This problem does not receive sufficient attention up to now. However, directed weighted networks are common in our daily life. For example, in a WeChat network, nodes denote users, and the weight of a directional edge from user a to user b means the number of messages sent from a to b ; in a friendship evaluating network, nodes denote member in a social system (like school, government, office, and club), and the weight of a directional edge from member a to member b means the grade of friendship that a thinks b as its friend; in a bipartite fans-actors Sina Weibo network, the weight of a directional edge from fans a to actor b means the number of fans a gives thumbs-up on the weblog of actor b in a period time. Perhaps the main reason that previous works ignore community detection in directed weighted networks is its complexity. To model directed weighted networks, benefited from the distribution-free idea of Qing (2021), the Directed Distribution-Free models (DiDFM) and its extension DiDCDFM were proposed by Qing and Wang (2022). DiDFM and DiDCDFM extend DFM and DCDFM from un-directed weighted networks to directed-weighted networks, respectively. SBM, DCSBM, ScBM, DCScBM, DFM, DCDFM and DiDFM can be seen as sub-models of DiDCDFM. However, though DiDFM and DiDCDFM are beautiful models, they can not model directed weighted networks in which nodes can belong to multiple communities. For overlapping directed weighted networks, the two-way blockmodels proposed in Airoidi et al. (2013) models directed weighted networks by allowing nodes to belong to more than one community and allowing edge weights to follow Normal or Bernoulli distribution. However, one main limitation of the two-way blockmodels is, it limits edge weights to follow Normal or Bernoulli distribution. Since bipartite networks allow row nodes to be different from column nodes and they contain directed

networks, we focus on modeling bipartite weighted networks. In this article, our goal is to close these gaps for bipartite weighted networks.

Main contributions of this paper are summarized as follows:

- a) We propose a novel model for bipartite weighted networks, the Bipartite Mixed Membership Distribution-Free (BiMMDF for short) model. BiMMDF can model a bipartite weighted network in which nodes can belong to multiple communities and edge weights can be any finite real values. In particular, bipartite signed networks in which nodes have mixed memberships can also be modeled by our BiMMDF. BiMMDF achieves its advantages by allowing elements of the adjacency matrix to follow arbitrary distribution as long as the expectation adjacency matrix has a block structure. MMSB, MMDF, DiMMSB and the two-way blockmodels are sub-models of BiMMDF. Some typical overlapping (and non-overlapping) networks can be modeled by our BiMMDF are sketched in Figure 1. We also conclude a brief comparison of previous models with our BiMMDF in Table 2.
- b) An efficient spectral algorithm is used to fit BiMMDF. This algorithm can exactly return true node memberships when applying the expectation adjacency matrix to replace the adjacency matrix as input, and this guarantees the identifiability of BiMMDF. A general theoretical guarantee on uniform rates of convergence for estimated node memberships returned by the algorithm is built under BiMMDF when the adjacency matrix comes from any distribution, where we also consider network sparsity parameter for our theoretical analysis. Meanwhile, theoretical upper bounds of error rates for a specific distribution can be immediately obtained from the general results.
- c) Separation conditions of a standard bipartite weighted network with two row (and column) communities for distributions like Bernoulli, Poisson, Binomial, Normal, Exponential, Uniform, Logistic, and bipartite signed network are obtained by delicate analysis under BiMMDF. For detail, see Examples 1-8. In particular, the separation condition of the Bernoulli distribution case is consistent with the classical results, and this guarantees the optimality of our theoretical results.
- d) The influence of the sparsity parameter on the algorithm’s performance and the behavior difference phenomenon on separation conditions of different distributions are verified by substantial computer-generated bipartite weighted networks. Numerical results of real-world directed weighted networks demonstrate the advantages of the algorithm in estimating node memberships, finding highly mixed nodes, and studying asymmetry between row and column communities.

2. The Bipartite Mixed Membership Distribution-Free model

The main symbols involved in this paper are summarized in Table 1. In this article, we propose a model that can model bipartite weighted networks in which nodes can belong to multiple communities.

Given a bipartite weighted network $\mathcal{N} = (\mathcal{V}_r, \mathcal{V}_c, \mathcal{W})$ with n_r row nodes and n_c column nodes, where $\mathcal{V}_r = \{1, 2, \dots, n_r\}$ is the set of row nodes, $\mathcal{V}_c = \{1, 2, \dots, n_c\}$ is the set of column nodes, and \mathcal{W} represents the set of edge weights. Let $A \in \mathbb{R}^{n_r \times n_c}$ be \mathcal{N} 's bi-adjacency matrix. In this paper, we allow $\mathcal{V}_r \neq \mathcal{V}_c$, i.e., row nodes can be different from column nodes and a bipartite setting case. We also allow $A(i, j)$ to be any finite real values for $i \in [n_r], j \in [n_c]$ because \mathcal{N} considered in this paper is a bipartite weighted network. In this article, we call \mathcal{N} directed weighted network when $\mathcal{V}_r = \mathcal{V}_c$ (i.e., row nodes are the same as column nodes) and call it a bipartite weighted network when $\mathcal{V}_r \neq \mathcal{V}_c$. Since a directed weighted network is a special case of a bipartite weighted network, we also call it a bipartite weighted network occasionally.

Symbol	Description	Symbol	Description
\mathbb{N}	Set of nonnegative integers	\mathbb{N}_+	Set of positive integers
\mathbb{R}	Set of real numbers	\mathbb{R}_+	Set of nonnegative real numbers
\mathcal{N}	Bipartite weighted network	\mathcal{V}_r	Set of row nodes
\mathcal{V}_c	Set of column nodes	$P \in \mathbb{R}^{K \times K}$	Block matrix
K	Number of row (column) communities	$\ x\ _q$	ℓ_q -norm for vector x
n_r	Number of row nodes	M'	Transpose of matrix M
n_c	Number of column nodes	$\mathbb{E}[M]$	Expectation of M
$A \in \mathbb{R}^{n_r \times n_c}$	\mathcal{N} 's adjacency matrix	$\ M\ _{2 \rightarrow \infty}$	Maximum ℓ_2 -norm of M
$\Pi_r \in [0, 1]^{n_r \times K}$	Membership matrix of row nodes	$M(i, :)$	i -th row of M
$\Pi_c \in [0, 1]^{n_c \times K}$	Membership matrix of column nodes	$M(:, j)$	j -th column of M
$[m]$	$\{1, 2, \dots, m\}$ for positive integer m	$M(S_r, :)$	Rows in the index set S_r of M
ρ	Sparsity parameter	$\text{rank}(M)$	Rank of M
$\sigma_k(M)$	k -th largest singular value of M	$\lambda_k(M)$	M 's k -th largest eigenvalue in magnitude
\mathcal{F}	Distribution	\mathcal{W}	Set of edge weights
$\Omega \in \mathbb{R}^{n_r \times n_c}$	A 's expectation matrix $\rho \Pi_r \Pi_c'$	$\kappa(M)$	Condition number of M
$U \in \mathbb{R}^{n_r \times K}$	Top K left singular vectors of Ω	$\mathcal{P}_r \in \{0, 1\}^{K \times K}$	Permutation matrix
$V \in \mathbb{R}^{n_c \times K}$	Top K right singular vectors of Ω	$\mathcal{P}_c \in \{0, 1\}^{K \times K}$	Permutation matrix
$\hat{U} \in \mathbb{R}^{n_r \times K}$	Top K left singular vectors of A	$ a $	Absolute value for real value a
$\hat{V} \in \mathbb{R}^{n_c \times K}$	Top K right singular vectors of A	e_i	$e_i(j) = 1(i = j)$
$\Lambda \in \mathbb{R}_+^{K \times K}$	Diagonal matrix of top K singular values of Ω	α_{in}	$\rho P(1, 1) = \alpha_{\text{in}} \frac{\log(n_r)}{n_r}$ when $K \geq 2$
$\hat{\Lambda} \in \mathbb{R}_+^{K \times K}$	Diagonal matrix of top K singular values of A	α_{out}	$\rho P(1, 2) = \alpha_{\text{out}} \frac{\log(n_r)}{n_r}$ when $K \geq 2$
$\hat{\Pi}_r \in [0, 1]^{n_r \times K}$	Estimated membership of row nodes	$\hat{\Pi}_c \in [0, 1]^{n_c \times K}$	Estimated membership of column nodes
τ	$\max_{i \in [n_r], j \in [n_c]} A(i, j) - \Omega(i, j) $	γ	$\max_{i \in [n_r], j \in [n_c]} \mathbb{E}((A(i, j) - \Omega(i, j))^2) / \rho$
$\text{diag}(M)$	Diagonal matrix with (i, i) -th entry $M(i, i)$	$\max(0, M)$	Matrix with (i, j) -th entry $\max(0, M(i, j))$
M^{-1}	Inverse of matrix M	I	Identity matrix of compatible dimension
η_r	Proportion of highly mixed row nodes	η_c	Proportion of highly mixed column nodes

Table 1: Main symbols of the paper.

For bipartite weighted network \mathcal{N} with mixed membership, our Bipartite Mixed Membership Distribution-Free model proposed in Definition 1 can model such \mathcal{N} with latent community structure.

Definition 1 Let $\Pi_r \in \mathbb{R}^{n_r \times K}$, $\Pi_c \in \mathbb{R}^{n_c \times K}$ such that $\text{rank}(\Pi_r) = K$, $\text{rank}(\Pi_c) = K$, $\Pi_r(i, k) \geq 0$, $\Pi_c(j, k) \geq 0$, $\|\Pi_r(i, :)\|_1 = 1$ and $\|\Pi_c(j, :)\|_1 = 1$ for $i \in [n_r]$, $j \in [n_c]$, $k \in [K]$, where $\Pi_r(i, :) \in \mathbb{R}^{K \times 1}$ and $\Pi_c(j, :) \in \mathbb{R}^{K \times 1}$ are the community membership vector for row node i and column node j , respectively. Let $P \in \mathbb{R}^{K \times K}$ satisfy $\max_{k, l \in [K]} |P(k, l)| = 1$ and $\text{rank}(P) = K$. Let $\rho > 0$ and call it sparsity parameter. Let $A \in \mathbb{R}^{n_r \times n_c}$ be the bi-adjacency matrix of a bipartite weighted network \mathcal{N} . For all pairs of (i, j) , our Bipartite Mixed Membership Distribution-Free (BiMMDF) model assumes that for arbitrary distribution \mathcal{F} , $A(i, j)$ are independent random variables generated from distribution \mathcal{F} satisfying

$$\mathbb{E}[A(i, j)] = \Omega(i, j), \text{ where } \Omega := \rho \Pi_r \Pi_c'. \quad (1)$$

For convenience, denote our model by $\text{BiMMDF}(n_r, n_c, K, P, \rho, \Pi_r, \Pi_c, \mathcal{F})$. Table 1 summaries sketches of different types of networks that can be modeled by our BiMMDF.

Remark 1 This remark provides some explanations and understandings on $K, \Pi_r, \Pi_c, P, \rho, \Omega$ and distribution \mathcal{F} under our model $\text{BiMMDF}(n_r, n_c, K, P, \rho, \Pi_r, \Pi_c, \mathcal{F})$.

- For K , it is the number of row communities and it is also the number of column communities. K considered in this paper is much smaller than $\min(n_r, n_c)$. When modeling a directed network in which both row and column nodes can belong to multiple communities, to make the model identifiable, the number of row communities must be the same as the number of column communities, where this conclusion is guaranteed by Proposition 1 in Qing and Wang (2021).
- For Π_r , it is the membership matrix for all row nodes. $\Pi_r(i, k)$ denotes the weight (which can also be seen as probability) of row node i on row community k for $i \in [n_r]$ and $k \in [K]$. Because weight is always nonnegative, $\Pi_r(i, k)$ is in the interval $[0, 1]$ in our model $\text{BiMMDF}(n_r, n_c, K, P, \rho, \Pi_r, \Pi_c, \mathcal{F})$. The probability of row node i belonging to all K row

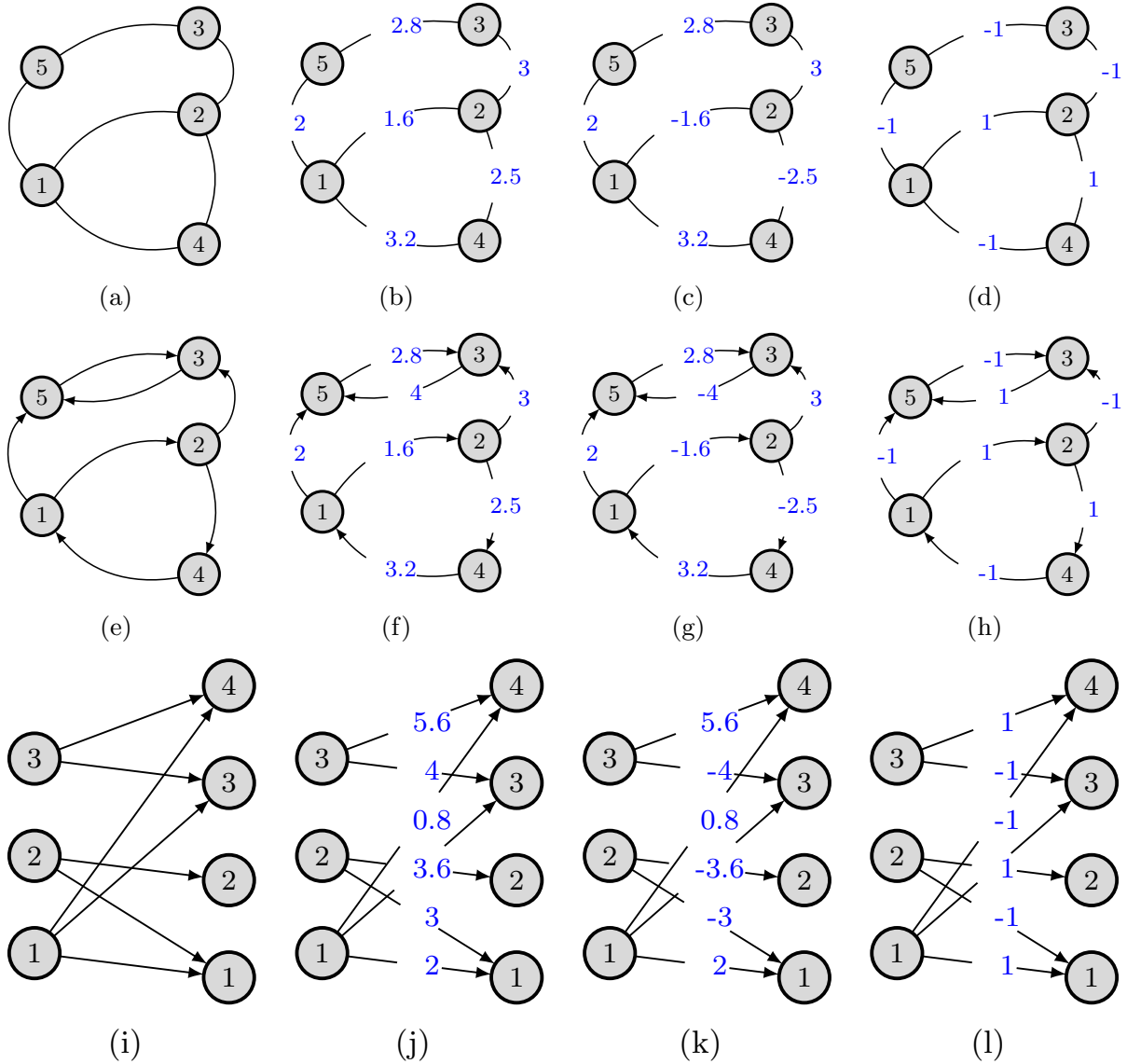


Figure 1: Illustrations for networks can be modeled by BiMMDF. Panel (a): un-directed un-weighted network. Panel (b): un-directed weighted network with positive weights. Panel (c): un-directed weighted network with positive and negative weights. Panel (d): un-directed signed network. Panel (e): directed un-weighted network. Panel (f): directed weighted network with positive weights. Panel (g): directed weighted network with positive and negative weights. Panel (h): directed signed network. Panel (i): bipartite un-weighted network. Panel (j): bipartite weighted network with positive weights. Panel (k): bipartite weighted network with positive and negative weights. Panel (l): bipartite signed network.

communities is 1, so BiMMDF requires $\sum_{k=1}^K \Pi_r(i, k) = 1$ for $i \in [n_r]$. Meanwhile, we require the rank of Π_r to be K because we need to make our model $\text{BiMMDF}(n_r, n_c, K, P, \rho, \Pi_r, \Pi_c, \mathcal{F})$ be identifiable. Similar explanations hold for Π_c . Furthermore, for models modeling networks with mixed membership (also known as overlapping) properties such that nodes can belong to multiple communities, membership matrix is a good way to denote nodes' memberships, see Airoldi et al. (2008, 2013); Jin et al. (2017); Mao et al. (2018, 2020); Zhang et al. (2020); Qing (2022c); Qing and Wang (2021).

- For P , it controls the block structure of $\mathbb{E}[A]$ (i.e., Ω) to make our model BiMMDF more applicable. Otherwise, if P is an identity matrix, we have $\mathbb{E}[A(i, j)] = \Omega(i, j) = \rho \Pi_r(i, :) \Pi_c'(j, :)$, which is much simpler than $\rho \Pi_r(i, :) P \Pi_c'(j, :)$. Therefore, considering P increases model popularity. Meanwhile, unlike models SBM, DCSBM, MMSB, ScBM, DCScBM, DCMM, and DiMMSB, ρP in our model BiMMDF is not a probability matrix unless \mathcal{F} is Bernoulli or Poisson or Binomial distribution because we allow P 's elements to be real values when \mathcal{F} is unknown. Therefore, whether P can have negative elements depends on distribution \mathcal{F} . For example, when \mathcal{F} is Bernoulli or Poisson or Binomial or some other distributions, all elements of P should be nonnegative or strictly positive, see Examples 1-3 and 5 for detail; when \mathcal{F} is Normal or Logistic or some other distributions, P 's elements can be any finite real values such that elements of adjacency matrix A generated from our model BiMMDF can also be any finite real values, see Examples 4 and 7 for detail. We set P 's maximum absolute element as 1 mainly for theoretical convenience because we consider the sparsity parameter ρ to control network sparsity. P is an asymmetric matrix, so BiMMDF can model bipartite weighted networks (sure, P can also be symmetric). Furthermore, we require the $K \times K$ matrix P to be full rank because we need our model BiMMDF well-defined and identifiable. For models (to name a few, MMSB, OCCAM, DCMM, DiMMSB, MMDF) modeling networks with overlapping properties, the $K \times K$ block matrix P must be full rank.
- For ρ , its range depends on distribution \mathcal{F} . For example, when \mathcal{F} is Bernoulli distribution such that ρP is a probability matrix, ρ should be in the interval $(0, 1]$ because $\max_{k, l \in [K]} |P(k, l)| = 1$; when \mathcal{F} is Poisson or Normal or Exponential or Logistic distribution, ρ can be set in $(0, +\infty)$. Meanwhile, when all entries of A are nonnegative, ρ controls network sparsity. However, when there exist negative elements in A , ρ does not control network sparsity. We call ρ sparsity parameter mainly for convenience and the fact that ρ controls network sparsity when A is the adjacency matrix of a directed un-weighted network. For a better understanding of ρ 's range and whether it controls network sparsity, please see Examples 1-8.
- For Ω , it is the expectation of A under our model BiMMDF and we also call it the population adjacency matrix. Benefitted from the fact that $\text{rank}(\Pi_r) = K, \text{rank}(\Pi_c) = K, \text{rank}(P) = K$ and K is much smaller than $\min(n_r, n_c)$, the rank of Ω is K by Equation (1). Therefore, we see that the $n_r \times n_c$ matrix Ω has a low-dimensional structure with only K nonzero singular values. We benefit a lot from Ω 's low-dimensional structure when we aim at designing a spectral algorithm to fit our model BiMMDF such that this algorithm can return Π_r and Π_c exactly when using Ω to replace A under BiMMDF.
- For distribution \mathcal{F} , it can be any distribution as long as Equation (1) holds. All entries of A generated from BiMMDF are directly related to distribution \mathcal{F} . For example, when \mathcal{F} is Bernoulli or Binomial distribution, A 's elements are nonnegative integers with an upper bound; when \mathcal{F} is Poisson distribution, A 's elements are nonnegative integers; when \mathcal{F} is Normal or Logistic distribution, A 's elements are real values; when \mathcal{F} is Uniform distribution, A 's elements are real values in a certain interval. Especially, we can generate bipartite signed networks from our BiMMDF such that A 's elements are either 1 or -1. For detail of these cases, see Examples 1-8. Note that it is possible that Equation (1) does not hold for some distributions. For example, \mathcal{F} can not be t -distribution because the mean of this distribution

is always 0; \mathcal{F} can not be Cauchy distribution because the mean of this distribution does not exist.

BiMMDF can be deemed as an extension of some previous models for networks in which nodes can belong to multiple communities.

- When \mathcal{F} is Bernoulli distribution such that all entries of A are either 1 or 0, BiMMDF reduces to DiMMSB Qing and Wang (2021), i.e., BiMMDF models bipartite weighted networks with mixed memberships while DiMMSB can only model bipartite un-weighted networks with mixed memberships, and DiMMSB is a sub-model of BiMMDF.
- When \mathcal{F} is Normal distribution, BiMMDF reduces to the two-way blockmodels proposed in Airoldi et al. (2013), i.e., BiMMDF can model bipartite weighted network in which elements of the adjacency matrix can be generated from more than Normal distribution while A 's entries are restricted to come from Normal distribution under the two-way blockmodels Airoldi et al. (2013), and the two-way blockmodels is a sub-model of BiMMDF.
- When $\Pi_r = \Pi_c, P = P'$ such that \mathcal{N} is an un-directed weighted network, BiMMDF degenerates to MMDF Qing (2022c), where MMDF only models un-directed weighted networks with overlapping property, and MMDF is a sub-model of BiMMDF.
- When $\Pi_r = \Pi_c, P = P'$ and \mathcal{F} is Bernoulli distribution, BiMMDF degenerates to MMSB Airoldi et al. (2008), where MMSB only models un-directed un-weighted networks with mixed memberships, and MMSB is a sub-model of BiMMDF.

Table 2 summaries comparisons of our BiMMDF with some previous SBM-based models. Note that in Table 2, if $\mathbb{E}[A]$ has a block structure like SBM under a model, spectral algorithms can be designed to fit such model since most spectral algorithms are designed by eigendecomposition or singular value decomposition of $\mathbb{E}[A]$. Since $\mathbb{E}[A] = \rho \Pi_r P \Pi_c'$ has a block structure under our BiMMDF, we will use a spectral algorithm to fit BiMMDF in this article.

Model	Adjacency matrix A	$\mathbb{E}[A]$ block	Distribution \mathcal{F}	Overlapping	Networks can be modeled
SBM Holland et al. (1983)	$A = A'$ and $A \in \{0, 1\}^{n \times n}$	Yes	Bernoulli	No	Panel (a) of Figure 1
MMSB Airoldi et al. (2008)	$A = A'$ and $A \in \{0, 1\}^{n \times n}$	Yes	Bernoulli	Yes	Panel (a) of Figure 1
DCSBM Karrer and Newman (2011)	$A = A'$ and $A \in \mathbb{N}^{n \times n}$	Yes	Bernoulli and Poisson	No	Panel (b) with nonnegative integer weights of Figure 1
OSBM Latouche et al. (2011)	$A = A'$ and $A \in \{0, 1\}^{n \times n}$	No	Bernoulli	No	Panels (a), (e) of Figure 1
Two-way blockmodels Airoldi et al. (2013)	$A \in \mathbb{R}^{n_r \times n_c}$	Yes	Normal and Bernoulli	Yes	Panels (a), (c), (e), (g), (i), (k) of Figure 1
WSBM Aicher et al. (2015)	$A = A', A \in \mathbb{R}^{n \times n}$	Yes	Exponential family	No	Panels (a)-(d) of Figure 1
ScBM Rohe et al. (2016)	$A \in \{0, 1\}^{n_r \times n_c}$	Yes	Bernoulli	No	Panels (a), (e), (i) of Figure 1
DCSBM Rohe et al. (2016)	$A \in \{0, 1\}^{n_r \times n_c}$	Yes	Bernoulli	No	Panels (a), (e), (i) of Figure 1
OCCAM Zhang et al. (2020)	$A = A'$ and $A \in \{0, 1\}^{n \times n}$	Yes	Bernoulli	Yes	Panel (a) of Figure 1
DCMM Jin et al. (2017)	$A = A'$ and $A \in \{0, 1\}^{n \times n}$	Yes	Bernoulli	Yes	Panel (a) of Figure 1
WSBM Palowitch et al. (2017)	$A = A'$ and $A \in \mathbb{R}_+^{n \times n}$	No	Distributions defined on \mathbb{R}_+	No	Panels (a), (b) of Figure 1
WSBMahn et al. (2018)	$A = A'$ and $A \in \mathbb{R}^{n \times n}$	Yes	Arbitrary	No	Panels (a)-(d) of Figure 1
SBMO Kaufmann et al. (2018)	$A = A'$ and $A \in \{0, 1\}^{n \times n}$	Yes	Bernoulli	Yes	Panel (a) of Figure 1
WSBM Xu et al. (2020)	$A = A'$ and $A \in \mathbb{R}^{n \times n}$	No	Arbitrary	No	Panels (a)-(d) of Figure 1
WMMSB Dulac et al. (2020)	$A = A'$ and $A \in \mathbb{N}^{n \times n}$	Yes	Poisson	Yes	Panel (b) with nonnegative integer weights of Figure 1
DiMMSB Qing and Wang (2021)	$A \in \{0, 1\}^{n_r \times n_c}$	Yes	Bernoulli	Yes	Panels (a), (e), (i) of Figure 1
WSBM Ng and Murphy (2021)	$A = A'$ and $A \in \mathbb{R}_+^{n \times n}$	No	Gamma	No	Panel (b) of Figure 1
DFM Qing (2021)	$A = A'$ and $A \in \mathbb{R}^{n \times n}$	Yes	Arbitrary	No	Panels (a)-(d) of Figure 1
DCDFM Qing (2022b)	$A = A'$ and $A \in \mathbb{R}^{n \times n}$	Yes	arbitrary	No	Panels (a)-(d) of Figure 1
MMDF Qing (2022c)	$A = A'$ and $A \in \mathbb{R}^{n \times n}$	Yes	Arbitrary	Yes	Panels (a)-(d) of Figure 1
DiDFM Qing and Wang (2022)	$A \in \mathbb{R}^{n_r \times n_c}$	Yes	Arbitrary	No	Panels (a)-(l) of Figure 1
DiDCDFM Qing and Wang (2022)	$A \in \mathbb{R}^{n_r \times n_c}$	Yes	Arbitrary	No	Panels (a)-(l) of Figure 1
BiMMDF (this paper)	$A \in \mathbb{R}^{n_r \times n_c}$	Yes	Arbitrary	Yes	Panels (a)-(l) of Figure 1

Table 2: Summary of SBM-based models, where $\mathbb{E}[A]$ block means that $\mathbb{E}[A]$ has a block structure like SBM.

Similar to Jin et al. (2017), call row node i ‘pure’ if $\Pi_r(i, :)$ degenerates (i.e., one entry is 1, all others $K - 1$ entries are 0) and ‘mixed’ otherwise. The same definitions hold for column nodes. In this article, we assume that for every $k \in [K]$, there exists at least one pure row node i such that $\Pi_r(i, k) = 1$ and at least one pure column node j such that $\Pi_c(j, k) = 1$, and these two assumptions are known as pure node assumption Jin et al. (2017); Mao et al. (2020, 2018); Zhang et al. (2020); Qing and Wang (2021). The requirements $\text{rank}(\Pi_r) = K$ and $\text{rank}(\Pi_c) = K$ in Definition 1 hold immediately as long as each row (column) community has at least one pure node. Since we assume that P is full rank and the pure node assumption holds, the distribution-free result Proposition

1 of Qing and Wang (2021) guarantees that BiMMDF is identifiable. Meanwhile, the conditions that P should be full rank and each row (column) cluster should have at least one pure node are necessary for the identifiability of models modeling network with mixed memberships, to name a few, MMSB Mao et al. (2020), DCMJ Jin et al. (2017); Mao et al. (2018), OCCAM Zhang et al. (2020) and DiMMSB Qing and Wang (2021).

3. A spectral algorithm for fitting the model

Since the rank of P is K , we have $\text{rank}(\Omega) = K$. Let $\Omega = U\Lambda V'$ be the top- K singular value decomposition (SVD) of Ω such that $U \in \mathbb{R}^{n_r \times K}$, $\Lambda \in \mathbb{R}_+^{K \times K}$, $V \in \mathbb{R}^{n_c \times K}$, $U'U = I$, $V'V = I$. Lemma 1 of Qing and Wang (2021) which is distribution-free guarantees the existences of simplex structures inherent in U and V , i.e., there exist two $K \times K$ matrices B_r and B_c such that $U = \Pi_r B_r$ and $V = \Pi_c B_c$. Similar to Mao et al. (2020), for simplex structures, applying the successive projection algorithm (SPA) Gillis and Vavasis (2015) to U (and V) with K row (and column) communities obtains B_r (and B_c). Thus, with given Ω , we can exactly return Π_r and Π_c by setting $\Pi_r = UB_r^{-1}$ and $\Pi_c = VB_c^{-1}$.

In practice, Ω is unknown but the adjacency matrix A is given and we aim at estimating Π_r and Π_c based on A . Recall that Ω is the expectation adjacency matrix of A and Ω 's rank is K under BiMMDF, we let $\hat{A} = \hat{U}\hat{\Lambda}\hat{V}'$ be the top- K SVD of A corresponding to the top- K singular values of A . We can see that $\hat{A}, \hat{U}, \hat{\Lambda}$ and \hat{V} can be seen as approximations of Ω, U, Λ and V , respectively. Then one should be able to obtain a good estimation of Π_r (and Π_c) by applying the SP algorithm on the rows of \hat{U} (and \hat{V}) assuming there are K row (and column) clusters. The spectral clustering algorithm we consider here to fit BiMMDF is summarized in Algorithm 1, which is the DiSP algorithm of Qing and Wang (2021) actually. In Algorithm 1, $\hat{\mathcal{L}}_r$ is the index set of pure nodes returned by SPA with input \hat{U} when there are K row communities. Similar explanation holds for $\hat{\mathcal{L}}_c$. Since BiMMDF can model a bipartite weighted network with mixed memberships, the input matrix of the DiSP algorithm considered here is the adjacency matrix of a bipartite weighted network. Meanwhile, the algorithm for fitting BiMMDF is the same as that of DiMMSB because DiSP enjoys the distribution-free property since Lemma 1 of Qing and Wang (2021) always holds without dependence on distribution \mathcal{F} .

Algorithm 1 DiSP

Require: Adjacency matrix $A \in \mathbb{R}^{n_r \times n_c}$ of a bipartite weighted network \mathcal{N} , number of row (and column) clusters K .

Ensure: $\hat{\Pi}_r$ and $\hat{\Pi}_c$.

- 1: Get the top- K SVD of A as $\hat{U}\hat{\Lambda}\hat{V}'$.
 - 2: $\hat{\mathcal{L}}_r = \text{SPA}(\hat{U})$ and $\hat{\mathcal{L}}_c = \text{SPA}(\hat{V})$.
 - 3: $\hat{B}_r = \hat{U}(\hat{\mathcal{L}}_r, :)$ and $\hat{B}_c = \hat{V}(\hat{\mathcal{L}}_c, :)$.
 - 4: $\hat{Y}_r = \hat{U}\hat{B}_r^{-1}$ and $\hat{Y}_c = \hat{V}\hat{B}_c^{-1}$.
 - 5: $\hat{Y}_r = \max(0, \hat{Y}_r)$ and $\hat{Y}_c = \max(0, \hat{Y}_c)$.
 - 6: $\hat{\Pi}_r = \text{diag}(\hat{Y}_r \mathbf{1}_K)^{-1} \hat{Y}_r$ and $\hat{\Pi}_c = \text{diag}(\hat{Y}_c \mathbf{1}_K)^{-1} \hat{Y}_c$.
-

3.1 Computational complexity

The time cost of DiSP mainly comes from the SVD step and the SPA step. The SVD step is also known as PCA Jin et al. (2017) and it is manageable even for a matrix with a large size. The complexity of SVD is $O(\max(n_r^2, n_c^2)K)$. The time cost of SPA is $O(\max(n_r, n_c)K^2)$ Jin et al. (2017). Since the number of clusters K is much smaller than n_r and n_c in this article, as a result, the total time cost of DiSP is $O(\max(n_r^2, n_c^2)K)$. Especially, when $n_r = O(n)$, $n_c = O(n)$ and $K = O(1)$, DiSP's complexity is $O(n^2)$. Meanwhile, DiSP can be seen as a directed version of the SPACL algorithm in Mao et al. (2020) which can process real-world networks of up to 100,000

nodes within tens of seconds. Therefore, DiSP inherits SPACL’s advantage such that it is easy to implement and computationally fast.

4. Main results for DiSP

In this section, we show the consistency of the algorithm, i.e., to show that the sample-based estimates $\hat{\Pi}_r$ and $\hat{\Pi}_c$ concentrate around the true mixed membership matrix Π_r and Π_c . Meanwhile, consistency is also known as consistent estimation, and it also means that the difference measured by some norms between the estimated membership matrix and the true membership matrix up to a permutation of labels goes to zero as the size of the network goes to infinity. Showing the consistency for spectral methods is common in community detection areas, see Qin and Rohe (2013); Jin (2015); Lei and Rinaldo (2015); Rohe et al. (2016); Jin et al. (2017); Mao et al. (2020); Zhang et al. (2020); Wang et al. (2020); Qing and Wang (2021). Similar to Mao et al. (2020), to build DiSP’s consistency under BiMMDF, we will provide a uniform rate of convergence for every node in this section. Throughout this paper, K is a known positive integer.

For theoretical convenience, we need the following assumptions and condition under BiMMDF to build a theoretical guarantee on DiSP’s error rates.

Assumption 1 *Assume that $\tau = \max_{i \in [n_r], j \in [n_c]} |A(i, j) - \Omega(i, j)|$ is finite.*

Assumption 2 *Assume that $\gamma = \frac{\max_{i \in [n_r], j \in [n_c]} \mathbb{E}[(A(i, j) - \Omega(i, j))^2]}{\rho}$ is finite.*

Assumption 3 *Assume that $\rho \gamma \max(n_r, n_c) \geq \tau^2 \log(n_r + n_c)$.*

Condition 1 *Assume that $\kappa(P) = O(1)$, $\frac{n_r}{n_c} = O(1)$, $\lambda_K(\Pi_r' \Pi_r) = O(\frac{n_r}{K})$ and $\lambda_K(\Pi_c' \Pi_c) = O(\frac{n_c}{K})$.*

Remark 2 *This remark provides some explanations on Assumptions 1-3 and Condition 1.*

- *Assumption 1 means that all entries of A and Ω should be finite, so this assumption is mild.*
- *Since $\Omega(i, j)$ is the expectation of $A(i, j)$ under our model BiMMDF, $\mathbb{E}[(A(i, j) - \Omega(i, j))^2]$ denotes the variance of $A(i, j)$. Therefore, Assumption 2 is also mild because it means that all variances of A ’s entries should be finite.*
- *The parameters γ and τ are directly related with distribution \mathcal{F} , and we will provide some examples to show that γ and τ are finite under different distribution \mathcal{F} in Examples 1-8.*
- *On the one hand, when A is generated from Bernoulli distribution (or some other distributions like Poisson or Binomial or Uniform or Exponential distribution) under BiMMDF such that all entries of A are nonnegative, Assumption 3 controls network sparsity for theoretical analysis. On the other hand, when A is generated from Normal distribution (or some other distributions like Logistic distribution or bipartite signed network) under BiMMDF such that some entries of A are nonnegative, Assumption 3 controls network size for theoretical analysis. Detailed analysis for Assumption 3 can be found in Examples 1-8 under different distribution \mathcal{F} . Meanwhile, when all entries of A are nonnegative, controlling network sparsity is common in community detection areas when building a theoretical guarantee on estimation consistency for some spectral methods. For example, theoretical upper bounds of error rates for spectral methods studied in Qin and Rohe (2013); Lei and Rinaldo (2015); Jin (2015); Rohe et al. (2016); Jin et al. (2017); Mao et al. (2020, 2018); Zhou and A. Amini (2019); Wang et al. (2020); Qing and Wang (2021) also depend on sparsity requirement similar to Assumption 3. Especially, when \mathcal{F} is Bernoulli distribution such that BiMMDF reduces to DiMMSB Qing and Wang (2021), the theoretical optimality of our requirement in Assumption 3 on network sparsity is guaranteed by the separation condition and sharp threshold criterion developed in Qing (2022a).*

- On the one hand, we use Condition 1 mainly for theoretical convenience when building Theorem 1 because it simplifies the theoretical upper bound of the row-wise singular vector when we use Theorem 4.4 Chen et al. (2021) to obtain our main theoretical results in Theorem 1. On the other hand, if we do not use Condition 1, the main results of theoretical upper bounds on DiSP's error rates under BiMMDF in Theorem 1 can also be obtained but with a more complex structure, for detail, please see the proof of Theorem 1. For comparison, Assumptions 1-3 are always required for theoretical analysis, and this is the reason that we do not call Condition 1 as an assumption. Meanwhile, in Condition 1, $\kappa(P) = O(1)$ means that P should be well-conditioned. $\frac{n_r}{n_c} = O(1)$ means that the number of row nodes should be in the same order as the number of column nodes. $\lambda_K(\Pi_r' \Pi_c) = O(\frac{n_r}{K})$ means that the "size" of each row community is in the same order and all row communities are nearly balanced. Same arguments hold for $\lambda_K(\Pi_c' \Pi_r) = O(\frac{n_c}{K})$. Condition 1 functions similar to Equations (2.14) and (2.15) of Jin et al. (2017) and conditions in Corollary 3.1 of Mao et al. (2020). Sure, Condition 1 contains the special case of SBM such that each community has an equal size.

Next theorem gives theoretical bounds on estimations of memberships for both row and column nodes, which is the main theoretical result for our DiSP method.

Theorem 1 Under $BiMMDF(n_r, n_c, K, P, \rho, \Pi_r, \Pi_c, \mathcal{F})$, let $\hat{\Pi}_r$ and $\hat{\Pi}_c$ be obtained from Algorithm 1, suppose Assumptions 1-3 and Condition 1 hold and $\sigma_K(\Omega) \gg \sqrt{\rho\gamma(n_r + n_c)\log(n_r + n_c)}$, with probability at least $1 - o((n_r + n_c)^{-5})$, for $i \in [n_r], j \in [n_c]$, we have

$$\|e'_i(\hat{\Pi}_r - \Pi_r \mathcal{P}_r)\|_1 = O\left(\frac{K^2 \sqrt{\gamma \log(n_r + n_c)}}{\sigma_K(P) \sqrt{\rho n_c}}\right), \|e'_j(\hat{\Pi}_c - \Pi_c \mathcal{P}_c)\|_1 = O\left(\frac{K^2 \sqrt{\gamma \log(n_r + n_c)}}{\sigma_K(P) \sqrt{\rho n_r}}\right).$$

Epecially, when $n_r = O(n), n_c = O(n)$, we have

$$\|e'_i(\hat{\Pi}_r - \Pi_r \mathcal{P}_r)\|_1 = O\left(\frac{K^2 \sqrt{\gamma \log(n)}}{\sigma_K(P) \sqrt{\rho n}}\right), \|e'_j(\hat{\Pi}_c - \Pi_c \mathcal{P}_c)\|_1 = O\left(\frac{K^2 \sqrt{\gamma \log(n)}}{\sigma_K(P) \sqrt{\rho n}}\right).$$

From Theorem 1, we see that our DiSP enjoys consistent estimation under our BiMMDF, i.e., theoretical upper bounds of DiSP's error rates go to zero as n_r and n_c go to infinity when P, K, ρ and distribution \mathcal{F} are fixed. Meanwhile, Theorem 1 also says that decreasing $\frac{\gamma}{\rho}$ improves DiSP's performances when n_r, n_c, K, Π_r and Π_c are fixed.

Epecially, under the same settings of Theorem 1, when $n_r = n_c = n$ and $K = O(1)$ (i.e., K is a small positive integer), Theorem 1 says that $\sigma_K(P)$ should shrink slower than $\sqrt{\frac{\gamma \log(n)}{\rho n}}$ for small error rates with high probability, where small error rates mean that theoretical upper bounds of error rates in Theorem 1 are very small and close to zero as long as $\sigma_K(P) \gg \sqrt{\frac{\gamma \log(n)}{\rho n}}$ when K, n, Π_r and Π_c are fixed. Next, we provide an analysis of small error rates with high probability for a standard bipartite weighted network.

For convenience, we need the following definition for our further theoretical analysis on a standard directed weighted network when $K = 2$.

Definition 2 Let $BiMMDF(n, 2, \Pi_r, \Pi_c, \alpha_{in}, \alpha_{out}, \mathcal{F})$ be a special case of $BiMMDF$ when $n_r = n_c = n, K = 2$, Condition 1 holds, and ρP has diagonal entries $p_{in} = \alpha_{in} \frac{\log(n)}{n}$ and non-diagonal entries $p_{out} = \alpha_{out} \frac{\log(n)}{n}$.

Since Π_r may not equal to Π_c and \mathcal{F} is not fixed, $BiMMDF(n, 2, \Pi_r, \Pi_c, \alpha_{in}, \alpha_{out}, \mathcal{F})$ still models a bipartite weighted network with row nodes has different memberships as column nodes though $n_r = n_c$. Note that since BiMMDF's identifiability requires P to be full rank, $|\alpha_{in}|$ should not equal to $|\alpha_{out}|$ under $BiMMDF(n, 2, \Pi_r, \Pi_c, \alpha_{in}, \alpha_{out}, \mathcal{F})$.

When the network is undirected (i.e., $\Pi_r = \Pi_c$), all nodes are pure, each community has equal size, and \mathcal{F} is Bernoulli distribution, $BiMMDF(n, 2, \Pi_r, \Pi_c, \alpha_{in}, \alpha_{out}, \mathcal{F})$ reduces to the SBM case

such that nodes connect with probability p_{in} within clusters and p_{out} across clusters (note that for SBM, since ρP is a probability matrix, p_{in} and p_{out} are nonnegative). This special case of SBM has been extensively and well studied in recent years, see Abbe et al. (2015); Abbe and Sandon (2015); Hajek et al. (2016); Abbe (2017) and references therein. Main finding in Abbe et al. (2015) says that exact recovery is possible if $|\sqrt{\alpha_{\text{in}}} - \sqrt{\alpha_{\text{out}}}| > \sqrt{2}$ and impossible if $|\sqrt{\alpha_{\text{in}}} - \sqrt{\alpha_{\text{out}}}| < \sqrt{2}$, where exact recovery means recovering the partition correctly with high probability when $n \rightarrow \infty$. For our BiMMDF, we are interested in the conditions α_{in} and α_{out} should satisfy such that DiSP's error rates are small with high probability under $\text{BiMMDF}(n, 2, \Pi_r, \Pi_c, \alpha_{\text{in}}, \alpha_{\text{out}}, \mathcal{F})$ when n is fixed, i.e., how small $|\alpha_{\text{in}}|, |\alpha_{\text{out}}|$ and $||\alpha_{\text{in}}| - |\alpha_{\text{out}}||$ can be to make DiSP's error rates be small with high probability for a fixed n . Unlike the concept of exact recovery studied in Abbe et al. (2015) which focuses on the case when $n \rightarrow \infty$, the concept of small error rates with high probability we consider in this paper focuses on the case when n is fixed. Note that since distribution \mathcal{F} is unknown for our $\text{BiMMDF}(n, 2, \Pi_r, \Pi_c, \alpha_{\text{in}}, \alpha_{\text{out}}, \mathcal{F})$, p_{in} and p_{out} (as well as α_{in} and α_{out}) may be negative.

Based on the theoretical upper bounds of error rates in Theorem 1, we have below corollary which provides requirements on α_{in} and α_{out} such that DiSP enjoys the property of small error rates with high probability under $\text{BiMMDF}(n, 2, \Pi_r, \Pi_c, \alpha_{\text{in}}, \alpha_{\text{out}}, \mathcal{F})$ when n is fixed and not too small.

Corollary 1 *Under $\text{BiMMDF}(n, 2, \Pi_r, \Pi_c, \alpha_{\text{in}}, \alpha_{\text{out}}, \mathcal{F})$, suppose Assumptions 1 and 2 hold, when n is not too small, with probability at least $1 - o(n^{-5})$, DiMISC's error rates are small and close to zero as long as*

$$\gamma \max(|\alpha_{\text{in}}|, |\alpha_{\text{out}}|) \geq \tau^2 + o(1) \text{ and } ||\alpha_{\text{in}}| - |\alpha_{\text{out}}|| \gg \tau. \quad (2)$$

Equation (2) means that, to make DiSP's error rates be small with high probability under BiMMDF, α_{in} and α_{out} should satisfy Equation (2). For convenience, we call Equation (2) separation condition.

Remark 3 *This remark provides some explanations on results in Corollary 1.*

- *Compared with Theorem 1, Corollary 1 does not need Assumption 3 and the lower bound requirement on $\sigma_K(\Omega)$ in Theorem 1 because these two conditions hold naturally as long as Equation (2) holds. For detail, please see the proof of Corollary 1. Meanwhile, the first and second inequalities in Equation 2 represent the same meanings as Assumption 3 and the lower bound requirement on $\sigma_K(\Omega)$, respectively, under the settings of $\text{BiMMDF}(n, 2, \Pi_r, \Pi_c, \alpha_{\text{in}}, \alpha_{\text{out}}, \mathcal{F})$.*
- *Under the settings of $\text{BiMMDF}(n, 2, \Pi_r, \Pi_c, \alpha_{\text{in}}, \alpha_{\text{out}}, \mathcal{F})$, the requirement $\kappa(P) = O(1)$ in Condition 1 holds immediately as long as Equation (2) holds. For detail, please see the proof of Corollary 1.*
- *In Corollary 1, the condition that n is not too small means n should be set much larger than 2. This condition on n mainly makes $\frac{\log(2n)}{\log(n)} = 1 + o(1)$ to make the requirements on α_{in} and α_{out} in Corollary 1 be concise. For detail, please see the proof of Corollary 1.*

It should be noted that the conditions on α_{in} and α_{out} for small error rates with high probability in Equation (2) closely depend on γ and τ where these two parameters are determined by distribution \mathcal{F} . Later we will provide more explicit conditions on α_{in} and α_{out} by analyzing τ and γ under different distribution \mathcal{F} . Based on Theorem 1, for all pairs (i, j) with $i \in [n_r], j \in [n_c]$, the following examples provide DiSP's error rates and explicit form of Equation (2) when A is generated under different distribution \mathcal{F} under our BiMMDF.

Example 1 *When \mathcal{F} is **Bernoulli distribution** such that $A(i, j) \sim \text{Bernoulli}(\Omega(i, j))$ for bipartite weighted network generated under BiMMDF, i.e., $A(i, j) \in \{0, 1\}$. For this case, BiMMDF degenerates to DiMMSB Qing and Wang (2021), where DiMMSB models bipartite un-weighted networks in which nodes can belong to multiple communities. For Bernoulli distribution, P should have*

nonnegative elements, $\mathbb{E}[A(i, j)] = \Omega(i, j)$ satisfying Equation (1), $\mathbb{P}(A(i, j) = 1) = \Omega(i, j)$, and $\frac{\mathbb{E}[(A(i, j) - \Omega(i, j))^2]}{\rho} = \frac{\Omega(i, j)(1 - \Omega(i, j))}{\rho} \leq \frac{\Omega(i, j)}{\rho} \leq 1$, so we have $\tau \leq 1$ and $\gamma \leq 1$, i.e., τ and γ are finite. Then, Assumption 3 means $\rho \geq \frac{\log(n_r + n_c)}{\max(n_r, n_c)}$. Therefore, for the Bernoulli distribution case, Assumption 3 controls network sparsity for our theoretical analysis. Setting γ as 1 in Theorem 1 obtains theoretical upper bounds of error rates of DiSP when \mathcal{F} is Bernoulli distribution and we see that increasing ρ decreases error rates. Meanwhile, using the four step separation condition and sharp threshold criterion developed in Qing (2022a), we find that our theoretical results are optimal. For the standard directed weighted network modeled by BiMMDF($n, 2, \Pi_r, \Pi_c, \alpha_{\text{in}}, \alpha_{\text{out}}, \mathcal{F}$), ρP is a probability matrix when \mathcal{F} is Bernoulli distribution, so ρ should be set in $(0, 1]$ since we require $\max_{k, l} |P(k, l)| = 1$, and α_{in} and α_{out} should be set in the interval $[0, \frac{n}{\log(n)}]$. Furthermore, setting $\gamma = 1$ and $\tau = 1$ in Equation (2) when \mathcal{F} is Bernoulli distribution, the more explicit condition on α_{in} and α_{out} is

$$\max(\alpha_{\text{in}}, \alpha_{\text{out}}) \geq 1 + o(1) \text{ and } |\alpha_{\text{in}} - \alpha_{\text{out}}| \gg 1. \quad (3)$$

Equation (3) says that for bipartite un-weighted network (i.e., the case when \mathcal{F} is Bernoulli distribution), to make DiSP's error rates be small with high probability, α_{in} (or α_{out}) should be set larger than 1 and the difference between α_{in} and α_{out} should be much larger than 1. By carefully analyzing Equation (3), we see that the first inequality always holds as long as the second inequality holds when \mathcal{F} is Bernoulli distribution. Unlike the exact recovery condition $|\sqrt{\alpha_{\text{in}}} - \sqrt{\alpha_{\text{out}}}| > \sqrt{2}$ developed in Abbe et al. (2015), DiSP's small error rates with high probability condition is $|\alpha_{\text{in}} - \alpha_{\text{out}}| \gg 1$ for bipartite un-weighted networks modeled by BiMMDF($n, 2, \Pi_r, \Pi_c, \alpha_{\text{in}}, \alpha_{\text{out}}, \mathcal{F}$).

Example 2 When \mathcal{F} is **Poisson distribution** such that $A(i, j) \sim \text{Poisson}(\Omega(i, j))$, i.e., $A(i, j) \in \mathbb{N}$. For Poisson distribution, P should have positive elements, $\mathbb{E}[A(i, j)] = \Omega(i, j)$ satisfying Equation (1), $\mathbb{P}(A(i, j) = m) = \frac{\Omega(i, j)^m}{m!} e^{-\Omega(i, j)}$ for any nonnegative integer m and $\mathbb{E}[(A(i, j) - \Omega(i, j))^2] = \Omega(i, j) \leq \rho$, so we have γ is finite and $\gamma \leq 1$. Therefore, for Poisson distribution, Assumption 3 means $\rho \geq \frac{\tau^2 \log(n_r + n_c)}{\max(n_r, n_c)}$ and it controls network sparsity. Setting γ as 1 in Theorem 1 obtains theoretical upper bounds of error rates of DiSP when \mathcal{F} is Poisson distribution and we find that increasing ρ decreases error rates. For τ , it is an unknown finite positive integer. Meanwhile, for this case, since ρP is not a probability matrix, ρ can be set in $(0, +\infty)$. For BiMMDF($n, 2, \Pi_r, \Pi_c, \alpha_{\text{in}}, \alpha_{\text{out}}, \mathcal{F}$) when \mathcal{F} is Poisson distribution, we see that α_{in} and α_{out} should be set in the interval $(0, +\infty)$. Furthermore, setting $\gamma = 1$ in Equation (2) when \mathcal{F} is Poisson distribution, the more explicit condition on α_{in} and α_{out} is

$$\max(\alpha_{\text{in}}, \alpha_{\text{out}}) \geq \tau^2 + o(1) \text{ and } |\alpha_{\text{in}} - \alpha_{\text{out}}| \gg \tau. \quad (4)$$

From Equation (4) obtained for the case when \mathcal{F} is Poisson distribution, we see that the condition that α_{in} and α_{out} should satisfy is stronger than that of Equation (3) obtained for the case when \mathcal{F} is Bernoulli distribution since τ is always much larger than 1 for Poisson distribution. We also see that for Poisson distribution, DiSP performs unsatisfactorily when the second inequality holds but the first inequality does not hold in Equation (4). When the second inequality holds, increasing $\max(\alpha_{\text{in}}, \alpha_{\text{out}})$ decreases DiSP's error rates. These phenomena are also verified by numerical results of simulations 1(b) and 2(b) in Section 5.1.

Example 3 When \mathcal{F} is **Binomial distribution** such that $A(i, j) \sim \text{Binomial}(m, \frac{\Omega(i, j)}{m})$ for any positive integer m , i.e., $A(i, j) \in \{0, 1, 2, \dots, m\}$. For Binomial distribution, all elements of P should be nonnegative, $\mathbb{E}[A(i, j)] = \Omega(i, j)$ satisfying Equation (1), and $\mathbb{E}[(A(i, j) - \Omega(i, j))^2] = m \frac{\Omega(i, j)}{m} (1 - \frac{\Omega(i, j)}{m}) = \Omega(i, j) (1 - \frac{\Omega(i, j)}{m}) \leq \rho$. So, $\tau = m$ and $\gamma \leq 1$. Then, Assumption 3 means $\rho \geq \frac{m^2 \log(n_r + n_c)}{\max(n_r, n_c)}$ and it controls network sparsity here. Setting γ as 1 in Theorem 1 gets theoretical upper bounds of error rates of DiSP when \mathcal{F} is Binomial distribution and we see that increasing ρ decreases error rates. Meanwhile, since $\frac{\Omega(i, j)}{m}$ is a probability, ρ should be less than m for this case.

For $\text{BiMMDF}(n, 2, \Pi_r, \Pi_c, \alpha_{\text{in}}, \alpha_{\text{out}}, \mathcal{F})$ when \mathcal{F} is Binomial distribution, α_{in} and α_{out} should be set in $(0, \frac{mn}{\log(n)}]$. Setting $\gamma = 1, \tau = m$ in Equation (2) when \mathcal{F} is Binomial distribution, we have

$$\max(\alpha_{\text{in}}, \alpha_{\text{out}}) \geq m^2 + o(1) \text{ and } |\alpha_{\text{in}} - \alpha_{\text{out}}| \gg m. \quad (5)$$

Note that when m is 1, Binomial distribution reduces to Bernoulli distribution, and we see that Equation (5) matches Equation (3). The analysis of Equation (5) for Binomial distribution is similar to Equation (4). The main difference between Equations (5) and (4) is: for numerical studies, τ is always a unknown large integer for Poisson distribution while m can be known for Binomial distribution. This difference is also verified by simulations 2(b), 3(c) and 3(d) in Section 5.1.

Example 4 When \mathcal{F} is **Normal distribution** such that $A(i, j) \sim \text{Normal}(\Omega(i, j), \sigma_A^2)$, i.e., $A(i, j) \in \mathbb{R}$, where σ_A^2 is the variance term of Normal distribution. For this case, BiMMDF reduces to the two-way blockmodels introduced in Airoidi et al. (2013). For Normal distribution, all elements of P are real values, $\mathbb{E}[A(i, j)] = \Omega(i, j)$ satisfying Equation (1), and $\mathbb{E}[(A(i, j) - \Omega(i, j))^2] = \sigma_A^2$. So, $\gamma = \frac{\sigma_A^2}{\rho}$ is finite. For τ , similar to the case for Poisson distribution, it is an unknown finite value. Then, Assumption 3 means $\frac{\sigma_A^2 \max(n_r, n_c)}{\log(n_r + n_c)} \geq \tau^2$. Therefore, for the Normal distribution case, Assumption 3 controls network size for our theoretical analysis, and this is different from Examples 1-3. Setting γ as $\frac{\sigma_A^2}{\rho}$ in Theorem 1 obtains theoretical upper bounds of error rates of DiSP when \mathcal{F} is Normal distribution and we see that increasing ρ (or decreasing σ_A^2) decreases error rates. Especially, when $\sigma_A^2 = 0$ such that $A = \Omega$, DiSP's error rates are zero. Meanwhile, for this case, ρ can be set in $(0, +\infty)$ because ρP is not a probability matrix and P can have negative elements. Therefore, for $\text{BiMMDF}(n, 2, \Pi_r, \Pi_c, \alpha_{\text{in}}, \alpha_{\text{out}}, \mathcal{F})$ when \mathcal{F} is Normal distribution, α_{in} and α_{out} should be set in $(-\infty, +\infty)$. Note that for $\text{BiMMDF}(n, 2, \Pi_r, \Pi_c, \alpha_{\text{in}}, \alpha_{\text{out}}, \mathcal{F})$, we have $\rho = \max(|p_{\text{in}}|, |p_{\text{out}}|) = \frac{\log(n)}{n} \max(|\alpha_{\text{in}}|, |\alpha_{\text{out}}|)$. Setting $\gamma = \frac{\sigma_A^2}{\rho} = \frac{\sigma_A^2 n}{\max(|\alpha_{\text{in}}|, |\alpha_{\text{out}}|) \log(n)}$ in Equation (2) when \mathcal{F} is Normal distribution, we have

$$\frac{\sigma_A^2 n}{\log(n)} \geq \tau^2 + o(1) \text{ and } ||\alpha_{\text{in}}| - |\alpha_{\text{out}}|| \gg \tau. \quad (6)$$

In Equation (6), the first inequality means a lower bound requirement on network size n . We see that when $\sigma_A^2 = 0$ such that $A = \Omega$, we have $\tau = 0$ and Equation (6) always holds naturally. We can also find that Equation (6) differs a lot from Equations (3)-(5) because α_{in} and α_{out} can be negative for Normal distribution. Note that Equation (6) has no requirement on $\max(|\alpha_{\text{in}}|, |\alpha_{\text{out}}|)$, which means that as long as $||\alpha_{\text{in}}| - |\alpha_{\text{out}}|| \gg \tau$, DiSP's error rates are small with high probability for Normal distribution. These phenomena are also verified by simulations 4(c) and 4(d) in Section 5.1.

Example 5 When \mathcal{F} is **Exponential distribution** such that $A(i, j) \sim \text{Exponential}(\frac{1}{\Omega(i, j)})$, i.e., $A(i, j) \in \mathbb{R}_+$. For Exponential distribution, all elements of P should be positive, $\mathbb{E}[A(i, j)] = \Omega(i, j)$ satisfying Equation (1), and $\mathbb{E}[(A(i, j) - \Omega(i, j))^2] = \Omega^2(i, j) \leq \rho^2$. So, $\gamma \leq \rho$ is finite. For τ , it is an unknown finite value. Therefore, for Exponential distribution, Assumption 3 means $\rho^2 \geq \frac{\tau^2 \log(n_r + n_c)}{\max(n_r, n_c)}$ and it controls network sparsity. Setting γ as ρ in Theorem 1 obtains theoretical upper bounds of DiSP's error rates when \mathcal{F} is Exponential distribution. Meanwhile, when setting γ as ρ in Theorem 1, ρ vanishes in the theoretical bounds, and this suggests that increasing ρ does not influence DiSP's error rates when \mathcal{F} is Exponential distribution (and this property is verified by simulation 5(a) in Section 5.1). For this case, ρ can be set in $(0, +\infty)$ since ρP is not a probability matrix. Therefore, for $\text{BiMMDF}(n, 2, \Pi_r, \Pi_c, \alpha_{\text{in}}, \alpha_{\text{out}}, \mathcal{F})$ when \mathcal{F} is Exponential distribution, α_{in} and α_{out} should be set in $(0, +\infty)$ because all elements of P are positive for Exponential distribution. Setting $\gamma = \rho = \max(|p_{\text{in}}|, |p_{\text{out}}|) = \frac{\log(n)}{n} \max(\alpha_{\text{in}}, \alpha_{\text{out}})$ in Equation (2) when \mathcal{F} is Exponential

distribution, we have

$$\max(\alpha_{\text{in}}^2, \alpha_{\text{out}}^2) \frac{\log(n)}{n} \geq \tau^2 + o(1) \text{ and } |\alpha_{\text{in}} - \alpha_{\text{out}}| \gg \tau. \quad (7)$$

Since the first inequality in Equation (7) depends on the term $\frac{\log(n)}{n}$, when n is large, Equation (7) has a more stronger requirement on $\max(\alpha_{\text{in}}, \alpha_{\text{out}})$ than that of Equations (3)-(6). Equation (7) means that even when the second inequality holds, to make DiSP's error rates be small with high probability (i.e., Equation (7) holds), $\max(\alpha_{\text{in}}, \alpha_{\text{out}})$ must be large enough to make the first inequality hold because of the $\frac{\log(n)}{n}$ term. This phenomenon is verified by simulations 5(b) and 5(c) in Section 5.1.

Example 6 When \mathcal{F} is **Uniform distribution** such that $A(i, j) \sim \text{Uniform}(0, 2\Omega(i, j))$, i.e., $A(i, j) \in (0, 2\rho)$. For Uniform distribution, all elements of P should be nonnegative, $\mathbb{E}[A(i, j)] = \frac{0+2\Omega(i, j)}{2} = \Omega(i, j)$ satisfying Equation (1), τ is no larger than 2ρ , and $\mathbb{E}[(A(i, j) - \Omega(i, j))^2] = \frac{4\Omega^2(i, j)}{12} \leq \frac{\rho^2}{3}$, i.e., $\gamma \leq \frac{\rho}{3}$ is finite. Therefore, for this case of Uniform distribution, Assumption 3 means $\rho^2 \geq \frac{3\tau^2 \log(n_r + n_c)}{\max(n_r, n_c)}$ and it controls network sparsity. Setting γ as $\frac{\rho}{3}$ in Theorem 1 obtains theoretical upper bounds of error rates for DiSP when \mathcal{F} is Uniform distribution. Since ρ vanishes in bounds of error rates when setting γ as $\frac{\rho}{3}$ in Theorem 1, increasing ρ has no influence on DiSP's performance (and this is verified by simulation 6(a) in Section 5.1). Meanwhile, ρ can be set in $(0, +\infty)$ since this case only requires that P should be nonnegative. Therefore, for BiMMDF($n, 2, \Pi_r, \Pi_c, \alpha_{\text{in}}, \alpha_{\text{out}}, \mathcal{F}$) when \mathcal{F} is Uniform distribution, α_{in} and α_{out} should be set in $[0, +\infty)$ because all elements of P are nonnegative for this case of Uniform distribution. Setting $\gamma = \rho/3 = \max(|p_{\text{in}}|, |p_{\text{out}}|)/3 = \frac{\log(n)}{3n} \max(\alpha_{\text{in}}, \alpha_{\text{out}})$ in Equation (2) when \mathcal{F} is Uniform distribution, we have

$$\max(\alpha_{\text{in}}^2, \alpha_{\text{out}}^2) \frac{\log(n)}{3n} \geq \tau^2 + o(1) \text{ and } |\alpha_{\text{in}} - \alpha_{\text{out}}| \gg \tau. \quad (8)$$

The analysis of Equation (8) is similar to Equation (7), and we omit it here. Unlike Bernoulli and Binomial distributions, τ is a random finite value though it has an upper bound of 2ρ for Uniform distribution, and this is the reason we still consider τ in Equation (8). Furthermore, we can also let $A(i, j) \sim \text{Uniform}(2\Omega(i, j), 0)$ such that $A(i, j) \in (-2\rho, 0)$, and for this case all elements of P should be negative (so α_{in} and α_{out} should be set in $(-\infty, 0]$, and α_{in} and α_{out} also satisfy Equation (8) by basic algebra). Furthermore, we can also use other forms of Uniform distribution, for example, $\text{Uniform}(u, 2\Omega(i, j) - u)$ or $\text{Uniform}(2\Omega(i, j) - u, u)$ for $\mu \in \mathbb{R}$ as long as Equation (1) holds when \mathcal{F} is Uniform distribution.

Example 7 When \mathcal{F} is **Logistic distribution** such that $A(i, j) \sim \text{Logistic}(\Omega(i, j), \beta)$, i.e., $A(i, j) \in \mathbb{R}$, where $\beta > 0$. For Logistic distribution, all elements of P are real values, $\mathbb{E}[A(i, j)] = \Omega(i, j)$ satisfying Equation (1), and $\mathbb{E}[(A(i, j) - \Omega(i, j))^2] = \frac{\pi^2 \beta^2}{3}$, i.e., $\gamma = \frac{\pi^2 \beta^2}{3\rho}$. Therefore, for Logistic distribution, Assumption 3 means $\frac{\pi^2 \beta^2 \max(n_r, n_c)}{3 \log(n_r + n_c)} \geq \tau^2$ and it controls network size for our theoretical analysis. Setting γ as $\frac{\pi^2 \beta^2}{3\rho}$ in Theorem 1 obtains theoretical upper bounds of DiSP's error rates, and we find that increasing ρ (or decreasing β) decreases error rates. Meanwhile, for this case, ρ can be set in $(0, +\infty)$. Therefore, for BiMMDF($n, 2, \Pi_r, \Pi_c, \alpha_{\text{in}}, \alpha_{\text{out}}, \mathcal{F}$) when \mathcal{F} is Logistic distribution, α_{in} and α_{out} can be set in $(-\infty, +\infty)$ because all elements of P are real values for Logistic distribution. Setting $\gamma = \frac{\pi^2 \beta^2}{3\rho} = \frac{\pi^2 \beta^2}{3 \max(|p_{\text{in}}|, |p_{\text{out}}|)} = \frac{\pi^2 \beta^2 n}{3 \max(|\alpha_{\text{in}}|, |\alpha_{\text{out}}|) \log(n)}$ in Equation (2) when \mathcal{F} is Logistic distribution, we have

$$\frac{\pi^2 \beta^2 n}{3 \log(n)} \geq \tau^2 + o(1) \text{ and } ||\alpha_{\text{in}}| - |\alpha_{\text{out}}|| \gg \tau. \quad (9)$$

The analysis of Equation (9) is similar to Equation (6), and we omit it here.

Example 8 *BiMMDF can also generate **bipartite signed networks** by setting $\mathbb{P}(A(i, j) = 1) = \frac{1+\Omega(i, j)}{2}$ and $\mathbb{P}(A(i, j) = -1) = \frac{1-\Omega(i, j)}{2}$, i.e., $A(i, j) \in \{-1, 1\}$. For bipartite signed networks, all elements of P are real values, $\mathbb{E}[A(i, j)] = \Omega(i, j)$ satisfying Equation (1), and $\mathbb{E}[(A(i, j) - \Omega(i, j))^2] = 1 - \Omega^2(i, j) \leq 1$, i.e., $\gamma \leq \frac{1}{\rho}$ is finite. For τ , it is finite with an upper bound of 2. Therefore, for bipartite signed network, Assumption 3 means $\frac{\max(n_r, n_c)}{\log(n_r + n_c)} \geq 4$ and it controls network size. Setting γ as $\frac{1}{\rho}$ in Theorem 1 obtains theoretical upper bounds of DiSP's error rates, and we see that increasing ρ decreases error rates. Meanwhile, for this case, ρ should be set in $(0, 1)$ because $\frac{1+\Omega(i, j)}{2}$ and $\frac{1-\Omega(i, j)}{2}$ are probabilities. Therefore, for $BiMMDF(n, 2, \Pi_r, \Pi_c, \alpha_{in}, \alpha_{out}, \mathcal{F})$ when $\mathbb{P}(A(i, j) = 1) = \frac{1+\Omega(i, j)}{2}$ and $\mathbb{P}(A(i, j) = -1) = \frac{1-\Omega(i, j)}{2}$ for bipartite signed network, α_{in} and α_{out} can be set in $(-\frac{n}{\log(n)}, \frac{n}{\log(n)})$ because all elements of P are real values. Setting $\gamma = \frac{1}{\rho} = \frac{1}{\max(|p_{in}|, |p_{out}|)} = \frac{1}{\max(|\alpha_{in}|, |\alpha_{out}|)\log(n)}$ and $\tau = 2$ in Equation (2) when \mathcal{F} is Logistic distribution, we have*

$$\frac{n}{\log(n)} \geq 4 + o(1) \text{ and } \|\alpha_{in}\| - \|\alpha_{out}\| \gg 2. \quad (10)$$

The analysis of Equation (10) is similar to Equation (6), and we omit it here.

Other choices of \mathcal{F} are also possible as long as Equation (1) holds under distribution \mathcal{F} for our BiMMDF. For example, \mathcal{F} can be set as Geometric, Laplace, and Gamma distributions in <http://www.stat.rice.edu/~dobelman/courses/texts/distributions.c&b.pdf>, where this link also provides details on probability mass function or probability density function for distributions in Examples 1-7.

5. Experimental Results

In this section, we present example applications of our method, first to computer-generated bipartite (and directed) weighted networks and then to real-world directed weighted networks.

5.1 Synthetic bipartite weighted networks

In this section, some simulations are conducted to investigate the performance of our DiSP. For computer-generated benchmark networks that contain known membership matrices Π_r and Π_c , our goal is to see whether and how accurately, the algorithm DiSP can estimate the memberships Π_r and Π_c . We measure DiSP's performance via Error Rate defined below:

$$\text{Error Rate} = \max\left(\frac{\min_{\mathcal{P} \in \mathcal{S}} \|\hat{\Pi}_r \mathcal{P} - \Pi_r\|_1}{n_r}, \frac{\min_{\mathcal{P} \in \mathcal{S}} \|\hat{\Pi}_c \mathcal{P} - \Pi_c\|_1}{n_c}\right),$$

where \mathcal{S} is the set of $K \times K$ permutation matrices. Since BiMMDF is the first model for bipartite weighted networks with overlapping property and DiSP is an algorithm specifically designed to fit BiMMDF such that DiSP can exactly recover Π_r and Π_c for the ideal case and DiSP enjoys consistent estimation under BiMMDF, DiSP has no competitors when estimating membership matrices for bipartite weighted networks generated under BiMMDF for different distribution \mathcal{F} .

For all simulations in this section, unless specified, the parameters $(n_r, n_c, K, P, \rho, \Pi_r, \Pi_c)$ and distribution \mathcal{F} under BiMMDF are set as follows. Set $K = 2$. Let each row block own $n_{r,0}$ number of pure nodes where the top $Kn_{r,0}$ row nodes $\{1, 2, \dots, Kn_{r,0}\}$ are pure and the rest row nodes $\{Kn_{r,0} + 1, Kn_{r,0} + 2, \dots, n_r\}$ are mixed with membership $(1/K, 1/K, \dots, 1/K)$. Similarly, let each column block own $n_{c,0}$ number of pure nodes where the top $Kn_{c,0}$ column nodes $\{1, 2, \dots, Kn_{c,0}\}$ are pure and column nodes $\{Kn_{c,0} + 1, Kn_{c,0} + 2, \dots, n_c\}$ are mixed with membership $(1/K, 1/K, \dots, 1/K)$. n_r, n_c, ρ and distribution \mathcal{F} are set independently for each experiment. For distribution (see, Bernoulli, Poisson, Binomial and Exponential distributions) which needs all elements of P be nonnegative, we set P as

$$P_1 = \begin{bmatrix} 1 & 0.2 \\ 0.3 & 0.8 \end{bmatrix}.$$

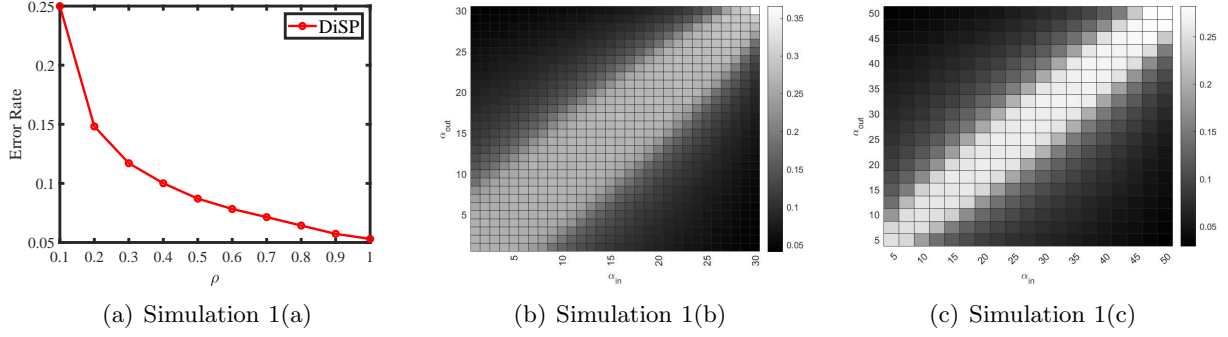


Figure 2: Bernoulli distribution. For panels (b) and (c): darker pixel represents lower Error Rate.

For distribution (see, Normal and Logistic distributions as well as bipartite signed network) which allows P to have negative elements, we set P as

$$P_2 = \begin{bmatrix} 1 & -0.2 \\ 0.3 & -0.8 \end{bmatrix}.$$

Meanwhile, when we consider the case $n_r = n_c = n$ for $BiMMDF(n, 2, \Pi_r, \Pi_c, \alpha_{in}, \alpha_{out}, \mathcal{F})$, we set ρP as

$$\tilde{P} = \begin{bmatrix} \alpha_{in} & \alpha_{out} \\ \alpha_{out} & \alpha_{in} \end{bmatrix} \frac{\log(n)}{n},$$

where we aim at changing α_{in} and α_{out} to investigate their influences on DiSP's performance and verify Equation (2) in Corollary 1 for different distribution \mathcal{F} .

Remark 4 *The only criteria for choosing the $K \times K$ matrix P is, P should be a full rank asymmetric (or symmetric) matrix, $\max_{k,l \in [K]} |P(k,l)| = 1$, and elements of P are positive or nonnegative or can be negative depending on distribution \mathcal{F} as analyzed in Experiments 1-8. The only criteria for setting Π_r and Π_c is, they should satisfy conditions in Definition 1, and there exist at least one pure row (and column) node for each row (and column) community.*

After obtaining P, ρ, Π_r , and Π_c , to generate a random adjacency matrix A with K row (and column) communities from distribution \mathcal{F} under our model BiMMDF, each simulation experiment contains the following steps:

- (a) Set $\Omega = \rho \Pi_r P \Pi_c'$.
- (b) Let $A(i, j)$ be a random number generated from distribution \mathcal{F} with expectation $\Omega(i, j)$ for $i \in [n_r], j \in [n_c]$.
- (c) Apply DiSP to A with K row (and column) communities. Record Error Rate.
- (d) Repeat (b)-(c) 50 times, and report the averaged error rates over the 50 repetitions.

We consider the following simulation setups.

5.1.1 BERNOULLI DISTRIBUTION

When $A(i, j) \sim \text{Bernoulli}(\Omega(i, j))$ for $i \in [n_r], j \in [n_c]$, by Example 1 we know that all entries of P should be nonnegative.

Simulation 1 (a): changing ρ . Let $n_r = 200, n_c = 300, n_{r,0} = 50, n_{c,0} = 100$ and P as P_1 . Since ρ should be set no larger than 1 for Bernoulli distribution, we let ρ range in $\{0.1, 0.2, 0.3, \dots, 1\}$. In panel (a) of Figure 2, we plot Error Rate against ρ . We see that DiSP performs better as ρ increases, and this matches analysis in Example 1.

Simulation 1 (b): changing α_{in} and α_{out} . Let $n = n_r = n_c = 300, n_{r,0} = 50, n_{c,0} = 100$ and ρP as \tilde{P} . Since \tilde{P} is a probability matrix for Bernoulli distribution, α_{in} and α_{out} should be set in $(0, \frac{n}{\log(n)}]$. For this simulation, we let α_{in} and α_{out} be in the range of $\{1, 2, 3, \dots, 30\}$,

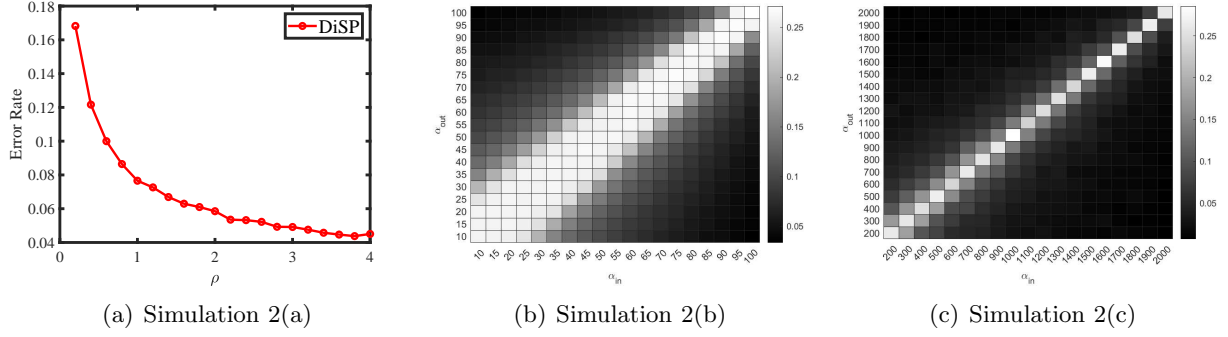


Figure 3: Poisson distribution. For panels (b) and (c): darker pixel represents lower Error Rate.

where $|\alpha_{in} - \alpha_{out}| \geq 1$ when $\alpha_{in} \neq \alpha_{out}$. The numerical results are shown in panel (b) of Figure 2. From the results, we see that DiSP’s error rates are large if $\max(\alpha_{in}, \alpha_{out})$ is too small even when $|\alpha_{in} - \alpha_{out}| \gg 1$ holds, and DiSP’s error rates are small if we increase $\max(\alpha_{in}, \alpha_{out})$ when $|\alpha_{in} - \alpha_{out}| \gg 1$ holds. These results are consistent with the small error rates with high probability condition on α_{in} and α_{out} provided in Equation (3).

Simulation 1 (c): changing α_{in} and α_{out} . All parameters are set the same as Simulation 1 (b) except that we let α_{in} and α_{out} be in the range of $\{5, 7.5, 10, 12.5, \dots, 50\}$ for this simulation, where $|\alpha_{in} - \alpha_{out}| \geq 2.5$ when $\alpha_{in} \neq \alpha_{out}$ (note that 2.5 is larger than 1 in Simulation 1 (b)). The numerical results are shown in panel (c) of Figure 2. We see that the “white” area (i.e., large error rates area of α_{in} and α_{out}) is narrower than that of panel (b). This suggests that when the first inequality of Equation (3) holds, increasing $|\alpha_{in} - \alpha_{out}|$ decreases DiSP’s error rates.

5.1.2 POISSON DISTRIBUTION

When $A(i, j) \sim \text{Poisson}(\Omega(i, j))$ for $i \in [n_r], j \in [n_c]$, by Example 2, all elements of P should be positive.

Simulation 2 (a): changing ρ . Let $n_r = 200, n_c = 300, n_{r,0} = 50, n_{c,0} = 100$ and P as P_1 . Since ρ can be set in $(0, +\infty)$ for Poisson distribution, we let ρ range in $\{0.2, 0.4, 0.6, \dots, 4\}$. The results are displayed in panel (a) of Figure 3. We see that increasing ρ decreases error rates, and this is consistent with findings in Experiment 2.

Simulation 2 (b): changing α_{in} and α_{out} . Let $n = n_r = n_c = 300, n_{r,0} = 50, n_{c,0} = 100$ and ρP as \tilde{P} . Since \tilde{P} is not a probability matrix for Poisson distribution and all entries of P should be positive, α_{in} and α_{out} can be set in $(0, +\infty)$. Here, we let α_{in} and α_{out} be in the range of $\{10, 15, 20, \dots, 100\}$, where $|\alpha_{in} - \alpha_{out}| \geq 5$ when $\alpha_{in} \neq \alpha_{out}$. The numerical results are shown in panel (b) of Figure 3. The analysis is similar to Simulation 1 (b), and we omit it here.

Simulation 2 (c): changing α_{in} and α_{out} . All parameters are set the same as Simulation 2 (b) except that we let α_{in} and α_{out} be in the range of $\{200, 300, 400, \dots, 2000\}$ for this simulation, where $|\alpha_{in} - \alpha_{out}| \geq 100$ when $\alpha_{in} \neq \alpha_{out}$. Panel (c) of Figure 3 shows the results. The analysis is similar to Simulation 1 (c), and we omit it here.

5.1.3 BINOMIAL DISTRIBUTION

When $A(i, j) \sim \text{Binomial}(m, \frac{\Omega(i, j)}{m})$ for any positive integer m for $i \in [n_r], j \in [n_c]$, by Example 3, all elements of P should be nonnegative and ρ should be set less than m .

Simulation 3 (a): changing ρ . Let $n_r = 200, n_c = 300, n_{r,0} = 50, n_{c,0} = 100, P$ be P_1 , and $m = 7$. Let ρ range in $\{0.2, 0.4, 0.6, \dots, 2\}$. Panel (a) of Figure 4 displays the results, and we see that DiSP’s error rates decrease when increasing ρ , which is consistent with the analysis in Experiment 3.

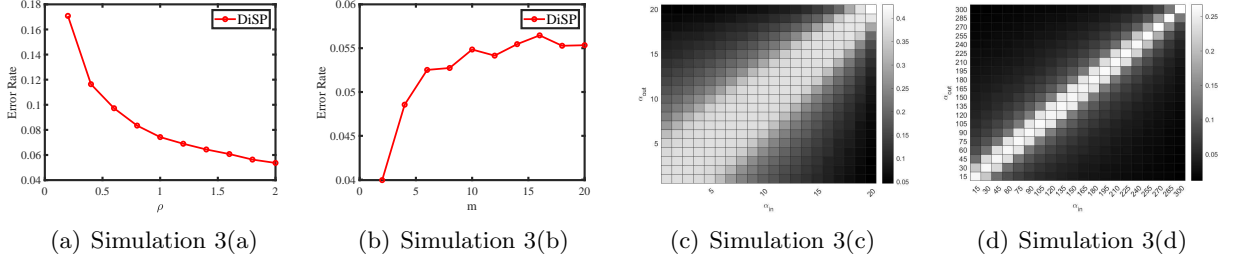


Figure 4: Binomial distribution. For panels (c) and (d): darker pixel represents lower Error Rate.

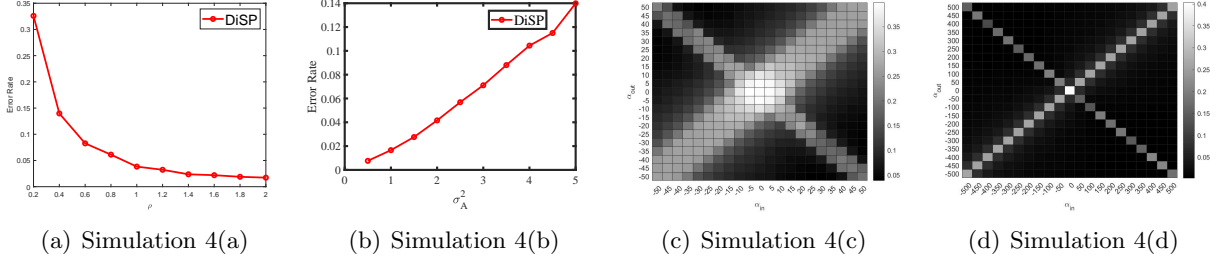


Figure 5: Normal distribution. For panels (c) and (d): darker pixel represents lower Error Rate.

Simulation 3 (b): changing m . Let $n_r = 200, n_c = 300, n_{r,0} = 50, n_{c,0} = 100$, P be P_1 , and $\rho = 2$. Let m range in $\{2, 4, 6, \dots, 20\}$. Panel (b) of Figure 4 show the results, and we see that increasing m increases error rates which is consistent with the analysis in Experiment 3.

Simulation 3 (c): changing α_{in} and α_{out} . Let $n = n_r = n_c = 300, n_{r,0} = 50, n_{c,0} = 100, m = 7$, and ρP as \tilde{P} . Since $\rho \leq m$ for Poisson distribution and $\rho = \frac{\log(n)}{n} \max(\alpha_{in}, \alpha_{out})$, α_{in} and α_{out} should be set in $(0, \frac{mn}{\log(n)}]$. For this simulation, we let α_{in} and α_{out} be in the range of $\{1, 2, 3, \dots, 20\}$, where $|\alpha_{in} - \alpha_{out}| \geq 1$ when $\alpha_{in} \neq \alpha_{out}$. Panel (c) of Figure 4 shows the results. The analysis is similar to Simulation 1 (b), and we omit it here.

Simulation 3 (d): changing α_{in} and α_{out} . All parameters are set the same as Simulation 3(b) except that we let α_{in} and α_{out} be in the range of $\{15, 30, 45, \dots, 300\}$ for this simulation, where $|\alpha_{in} - \alpha_{out}| \geq 15$ when $\alpha_{in} \neq \alpha_{out}$. Panel (d) of Figure 3 shows the results. The analysis is similar to Simulation 1 (c), and we omit it here.

5.1.4 NORMAL DISTRIBUTION

When $A(i, j) \sim \text{Normal}(\Omega(i, j), \sigma_A^2)$ for some $\sigma_A^2 > 0$ for $i \in [n_r], j \in [n_c]$, by Example 4, all elements of P are real values and ρ can be set in $(0, +\infty)$.

Simulation 4 (a): changing ρ . Let $n_r = 200, n_c = 300, n_{r,0} = 50, n_{c,0} = 100$, P be P_2 , and $\sigma_A^2 = 1$. Let ρ range in $\{0.2, 0.4, 0.6, \dots, 2\}$. The results are shown in panel (a) of Figure 5. We see that DiSP's error rates decrease when ρ increases, and this is consistent with findings in Experiment 4.

Simulation 4 (b): changing σ_A^2 . Let $n_r = 200, n_c = 300, n_{r,0} = 50, n_{c,0} = 100$, P be P_2 , and $\rho = 2$. Let σ_A^2 range in $\{0.5, 1, 1.5, \dots, 5\}$. The results are displayed in panel (b) of Figure 5. We see that DiSP's error rates increases when σ_A^2 increases, and this is consistent with the analysis in Experiment 4.

Simulation 4 (c): changing α_{in} and α_{out} . Let $n = n_r = n_c = 300, n_{r,0} = 50, n_{c,0} = 100, \sigma_A^2 = 1$, and ρP as \tilde{P} . Since ρ can be set in $(0, +\infty)$ and all entries of P can be negative for Normal distribution, and $\rho = \frac{\log(n)}{n} \max(|\alpha_{in}|, |\alpha_{out}|)$, α_{in} and α_{out} can be set in $(-\infty, +\infty)$. For this simulation, we let α_{in} and α_{out} be in the range of $\{-50, -45, -40, \dots, 50\}$, where $||\alpha_{in}| - |\alpha_{out}|| \geq 15$ when $|\alpha_{in}| \neq |\alpha_{out}|$. Panel (c) of Figure 5 shows the results. Because the first inequality of Equation (6) does not add constraint on $\max(|\alpha_{in}|, |\alpha_{out}|)$, DiSP's error rates are small as long as the second

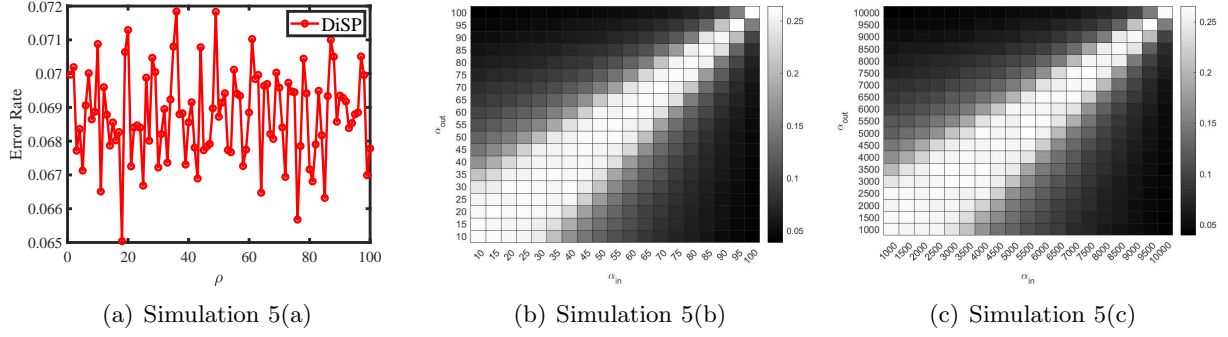


Figure 6: Exponential distribution. For panels (b) and (c): darker pixel represents lower Error Rate.

inequality holds. We see that results of Simulation 4 (c) support Equation (6) because the “white” area in panel (c) of Figure 5 enjoys a symmetric structure while the “white” areas in panel (b) of Figure 2, panel (b) of Figure 3 and panel (c) of Figure 4 have an asymmetric structure because the first inequality of Equations (3)-(5) has requirement on $\max(\alpha_{in}, \alpha_{out})$.

Simulation 4 (d): changing α_{in} and α_{out} . All parameters are set the same as Simulation 4(c) except that we let α_{in} and α_{out} be in the range of $\{-500, -450, -400, \dots, 500\}$ for this simulation, where $||\alpha_{in}| - |\alpha_{out}|| \geq 150$ when $|\alpha_{in}| \neq |\alpha_{out}|$ (note that 150 is much larger than 15 in Simulation 4 (c)). The results are displayed in panel (d) of Figure 5. Error rates of Simulation 4 (d) are much smaller than that of Simulation 4 (c) because we increase $||\alpha_{in}| - |\alpha_{out}||$ when $|\alpha_{in}| \neq |\alpha_{out}|$. So, results of this simulation also support Equation (6).

5.1.5 EXPONENTIAL DISTRIBUTION

When $A(i, j) \sim \text{Exponential}(\frac{1}{\Omega(i, j)})$ for $i \in [n_r], j \in [n_c]$, by Example 5, P should have positive entries. and ρ can be set in $(0, +\infty)$.

Simulation 5 (a): changing ρ . Let $n_r = 200, n_c = 300, n_{r,0} = 50, n_{c,0} = 100$, P be P_1 . Let ρ range in $\{1, 2, 3, \dots, 100\}$. In the plot of the result (Figure 6 (a)), we see that increasing ρ has no influence on DiSP’s performance, and this phenomenon matches our findings in Example 5 because ρ vanishes in the theoretical upper bounds of error rates when setting γ as ρ for Exponential distribution.

Simulation 5 (b): changing α_{in} and α_{out} . Let $n = n_r = n_c = 300, n_{r,0} = 50, n_{c,0} = 100$ and ρP as \tilde{P} . Since \tilde{P} is not a probability matrix for Exponential distribution and all entries of P should be positive, α_{in} and α_{out} can be set in $(0, +\infty)$. Here, we let α_{in} and α_{out} be in the range of $\{10, 15, 20, \dots, 100\}$, where $|\alpha_{in} - \alpha_{out}| \geq 5$ when $\alpha_{in} \neq \alpha_{out}$. The numerical results are shown in panel (b) of Figure 6. We see that the “white” area of panel (b) has an asymmetric structure, and this phenomenon occurs because $\max(\alpha_{in}, \alpha_{out})$ should be sufficiently large to make DiSP’s error rates be small even when the second inequality of Equation (7) holds.

Simulation 5 (c): changing α_{in} and α_{out} . All parameters are set the same as Simulation 5(b) except that we let α_{in} and α_{out} be in the range of $\{1000, 1500, 2000, \dots, 10000\}$ for this simulation, where $|\alpha_{in} - \alpha_{out}| \geq 500$ when $\alpha_{in} \neq \alpha_{out}$ (note that 500 is much larger than 5 in Simulation 5 (b)). The results are displayed in panel (c) of Figure 6. Unlike Simulations 1-4, the “white” area in panel (c) of Figure 6 still has an asymmetric structure even though 500 is much larger than 5. This phenomenon occurs because the first inequality of Equation (7) is $\max(\alpha_{in}^2, \alpha_{out}^2) \frac{\log(n)}{n} \geq \tau^2 + o(1)$. The $\frac{\log(n)}{n}$ term makes that to make Equation (7) hold, $\max(\alpha_{in}, \alpha_{out})$ must be large enough even when the second inequality of Equation (7) holds. Therefore, the asymmetric structures of “white” areas in panel (b) and (c) of Figure 6 support our findings in Equation (7) for Exponential distribution.

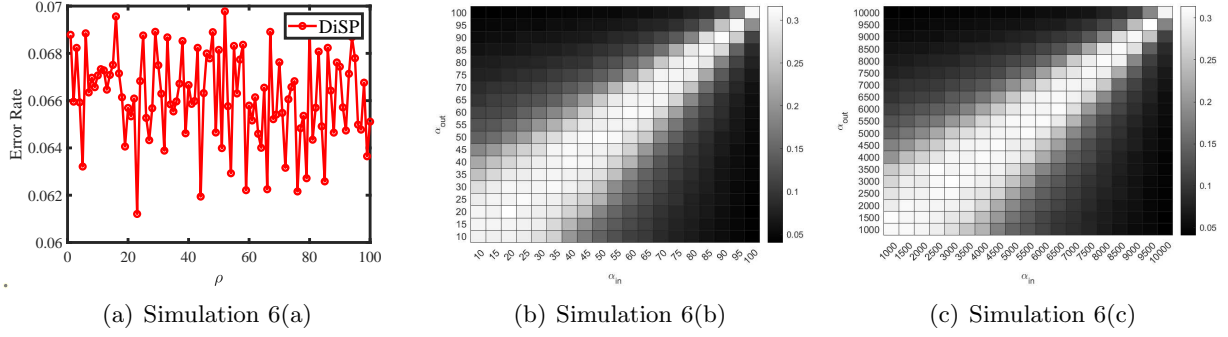


Figure 7: Uniform distribution. For panels (b) and (c): darker pixel represents lower Error Rate.

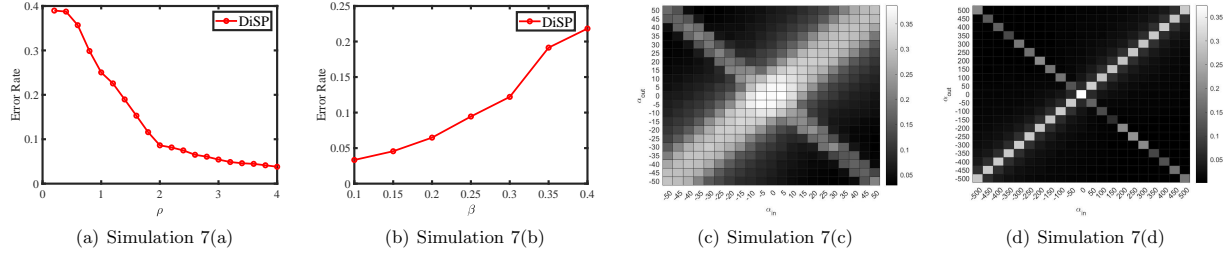


Figure 8: Logistic distribution. For panels (c) and (d): darker pixel represents lower Error Rate.

5.1.6 UNIFORM DISTRIBUTION

When $A(i, j) \sim \text{Uniform}(0, 2\Omega(i, j))$ for $i \in [n_r], j \in [n_c]$, by Example 6, all entries of P should be nonnegative and ρ can be set in $(0, +\infty)$.

Simulation 6 (a): changing ρ . Let $n_r = 30, n_c = 50, n_{r,0} = 10, n_{c,0} = 20$, P be P_1 . Let ρ range in $\{1, 2, 3, \dots, 100\}$. Panel (a) of Figure 7 shows the results. We see that ρ has no influence on DiSP's error rates for Uniform distribution, and this verifies our findings in Experiment 6.

Simulation 6 (b): changing α_{in} and α_{out} . Let $n = n_r = n_c = 50, n_{r,0} = 10, n_{c,0} = 20$ and ρP as \tilde{P} . Since \tilde{P} is not a probability matrix for Uniform distribution and all entries of P should be positive, α_{in} and α_{out} can be set in $(0, +\infty)$ when $A(i, j) \sim \text{Uniform}(0, 2\Omega(i, j))$ for $i \in [n_r], j \in [n_c]$. Here, we let α_{in} and α_{out} be in the range of $\{10, 15, 20, \dots, 100\}$. The numerical results are shown in panel (b) of Figure 7. The analysis for this simulation is similar to that of Simulation 5 (b), and we omit it here.

Simulation 6 (c): changing α_{in} and α_{out} . All parameters are set the same as Simulation 6(b) except that we let α_{in} and α_{out} be in the range of $\{1000, 1500, 2000, \dots, 10000\}$ for this simulation. The numerical results are displayed in panel (c) of Figure 7. The analysis is similar to that of Simulation 5 (c), and we omit it here.

5.1.7 LOGISTIC DISTRIBUTION

When $A(i, j) \sim \text{Logistic}(\Omega(i, j), \beta)$ for $\beta > 0$ for $i \in [n_r], j \in [n_c]$, by Example 7, all entries of P are real values and ρ can be set in $(0, +\infty)$.

Simulation 7(a): changing ρ . Let $n_r = 30, n_c = 50, n_{r,0} = 10, n_{c,0} = 20, \beta = 1$ and P be P_2 . Let ρ range in $\{0.2, 0.4, 0.6, \dots, 4\}$.

Simulation 7 (b): changing β . Let $n_r = 30, n_c = 50, n_{r,0} = 10, n_{c,0} = 20, \rho = 0.5$, and P be P_2 . Let β range in $\{0.1, 0.15, 0.2, \dots, 0.4\}$.

Simulation 7 (c): changing α_{in} and α_{out} . Let $n = n_r = n_c = 50, n_{r,0} = 10, n_{c,0} = 20, \beta = 1$, and ρP as \tilde{P} . Since ρ can be set in $(0, +\infty)$ and all entries of P are real values for Logistic

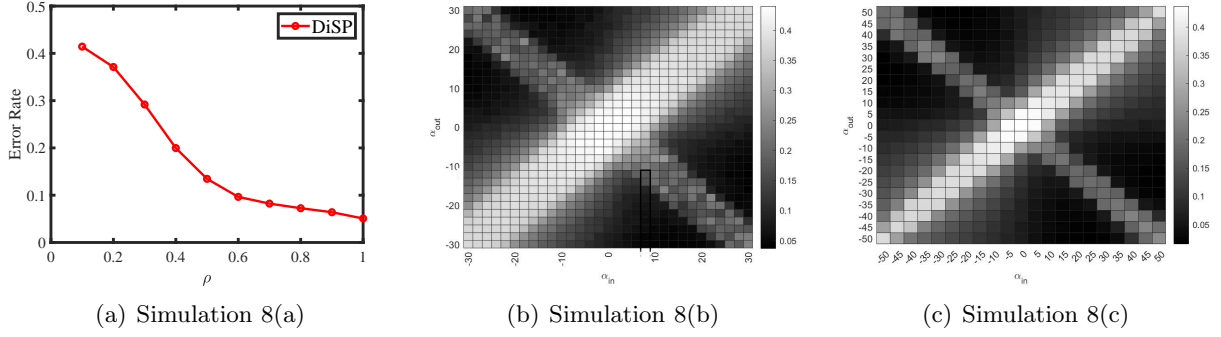


Figure 9: Bipartite signed network. For panels (b) and (c): darker pixel represents lower Error Rate.

distribution, α_{in} and α_{out} can be set in $(-\infty, +\infty)$. For this simulation, we let α_{in} and α_{out} be in the range of $\{-50, -45, -40, \dots, 50\}$.

Simulation 7 (d): changing α_{in} and α_{out} . All parameters are set the same as Simulation 7(c) except that we let α_{in} and α_{out} be in the range of $\{-500, -450, -400, \dots, 500\}$ for this simulation.

Panels (a)-(d) of Figure 8 display results of Simulations 7 (a)-(d), respectively. The analysis is similar to that of Simulation 4, and we omit it here.

5.1.8 BIPARTITE SIGNED NETWORK

For bipartite signed network when $\mathbb{P}(A(i, j) = 1) = \frac{1+\Omega(i, j)}{2}$ and $\mathbb{P}(A(i, j) = -1) = \frac{1-\Omega(i, j)}{2}$ for $i \in [n_r], j \in [n_c]$, by Example 8, P 's entries are real values and ρ should be set in $(0, 1)$.

Simulation 8 (a): changing ρ . Let $n_r = 100, n_c = 150, n_{r,0} = 30, n_{c,0} = 60$ and P be P_2 . Let ρ range in $\{0.1, 0.2, 0.3, \dots, 1\}$.

Simulation 8 (b): changing α_{in} and α_{out} . Let $n = n_r = n_c = 300, n_{r,0} = 100, n_{c,0} = 120$ and ρP as \tilde{P} . Since P can have negative values and $\rho \in (0, 1)$ for directed signed network, α_{in} and α_{out} can be set in $(-\frac{n}{\log(n)}, \frac{n}{\log(n)})$. For this simulation, we let α_{in} and α_{out} be in the range of $\{-30, -28, -26, \dots, 30\}$. The numerical results are shown in panel (b) of Figure 9.

Simulation 8 (c): changing α_{in} and α_{out} . All parameters are set the same as Simulation 8(b) except that we let α_{in} and α_{out} be in the range of $\{-50, -45, -40, \dots, 50\}$. The numerical results are shown in panel (c) of Figure 9.

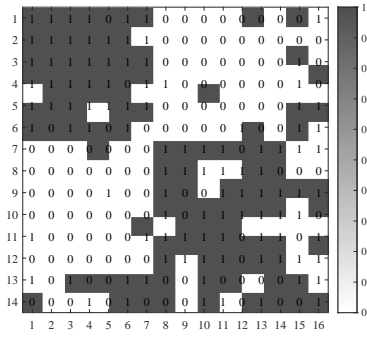
Panels (a)-(c) of Figure 9 display results of Simulations 8 (a)-(c), respectively. The analysis is similar to that of Simulations 4(a), 4(c), and 4(d), and we omit it here.

Remark 5 For visuality, we plot adjacency matrices of bipartite weighted networks generated under BiMMDF for different distribution \mathcal{F} in this remark. For P , we set it as below two cases:

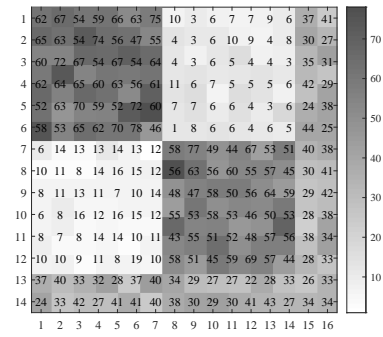
$$P_a = \begin{bmatrix} 1 & 0.2 \\ 0.1 & 0.9 \end{bmatrix} \text{ or } P_b = \begin{bmatrix} 1 & -0.2 \\ 0.1 & -0.9 \end{bmatrix}.$$

Under different \mathcal{F} , ρ should be set in the interval obtained in Examples 1-8. We consider below eight settings.

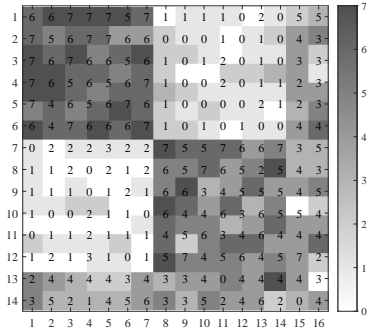
Model set-up 1: When $A(i, j) \sim \text{Bernoulli}(\Omega(i, j))$ for $i \in [n_r], j \in [n_c]$, set $n_r = 16, n_{r,0} = 7, n_c = 14, n_{c,0} = 6, \rho = 0.9$ and P as P_a . For this set-up, a bipartite un-weighted network with 16 row nodes and 14 column nodes is generated from BiMMDF. Panel (a) of Figure 10 shows an adjacency matrix A generated under BiMMDF for model set-up 1, where we also report DiSP's error rate. With given A and known memberships Π_r and Π_c for this set-up, readers can apply DiSP to A to check the effectiveness of DiSP.



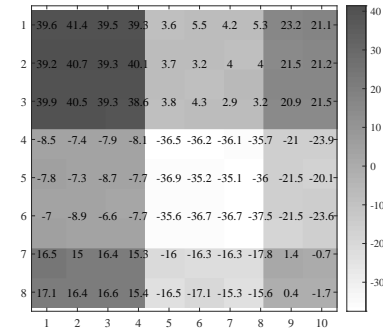
(a) A of model set-up 1



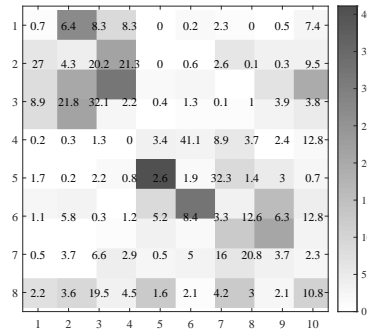
(b) A of model set-up 2



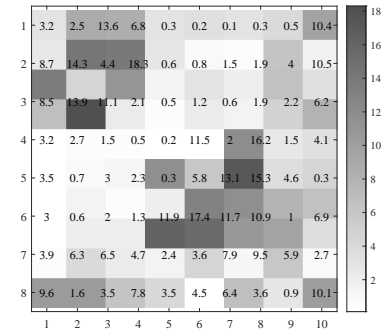
(c) A of model set-up 3



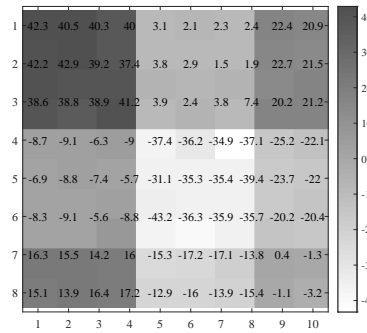
(d) A of model set-up 4



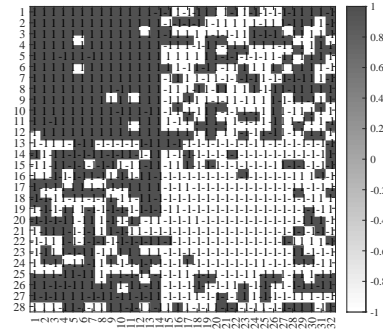
(e) A of model set-up 5



(f) A of model set-up 6



(g) A of model set-up 7



(h) A of model set-up 8

Figure 10: Illustration for bipartite weighted networks' adjacency matrices generated under BiM-MDF. For A in panel (a)-(h), DiSP's Error Rates are 0.0266, 0.0055, 0.0036, 0.0011, 0.0755, 0.0348, 0.0015, and 0.0552, respectively. In panels (d)-(g), we keep A 's elements in one decimal for visualization beauty.

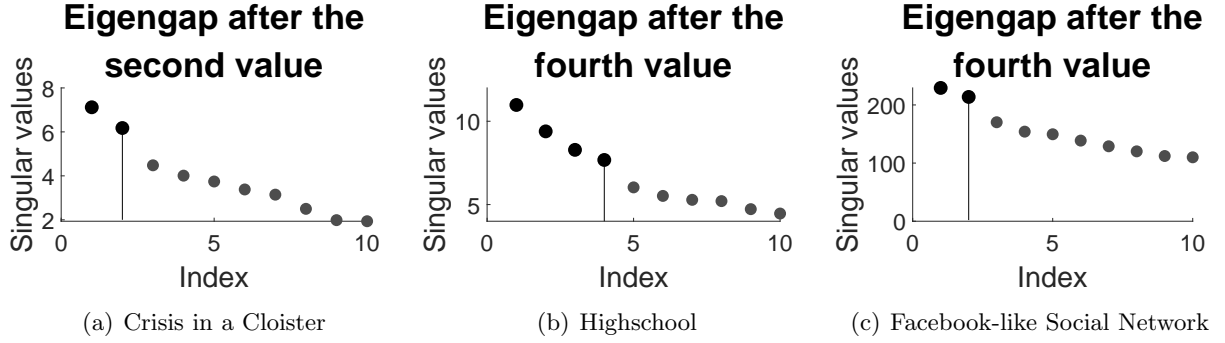


Figure 11: Top 10 singular values of A for real-world directed weighted networks used in this paper.

Model set-up 2: When $A(i, j) \sim \text{Poisson}(\Omega(i, j))$ for $i \in [n_r], j \in [n_c]$, set $n_r = 16, n_{r,0} = 7, n_c = 14, n_{c,0} = 6, \rho = 60$ and P as P_a . Panel (b) of Figure 10 shows an adjacency matrix A generated under BiMMDF for this set-up.

Model set-up 3: When $A(i, j) \sim \text{Binomial}(m, \Omega(i, j)/m)$ for $i \in [n_r], j \in [n_c]$, set $n_r = 16, n_{r,0} = 7, n_c = 14, n_{c,0} = 6, m = 7, \rho = 6$ and P as P_a . Panel (c) of Figure 10 shows an adjacency matrix A generated under BiMMDF for this set-up.

Model set-up 4: When $A(i, j) \sim \text{Normal}(\Omega(i, j), \sigma_A^2)$ for $i \in [n_r], j \in [n_c]$, set $n_r = 10, n_{r,0} = 4, n_c = 8, n_{c,0} = 3, \sigma_A^2 = 1, \rho = 40$ and P as P_b . Panel (d) of Figure 10 shows an adjacency matrix A generated under BiMMDF for this set-up.

Model set-up 5: When $A(i, j) \sim \text{Exponential}(\frac{1}{\Omega(i, j)})$ for $i \in [n_r], j \in [n_c]$, set $n_r = 10, n_{r,0} = 4, n_c = 8, n_{c,0} = 3, \rho = 10$ and P as P_a . Panel (e) of Figure 10 shows an adjacency matrix A generated under BiMMDF for this set-up.

Model set-up 6: When $A(i, j) \sim \text{Uniform}(0, 2\Omega(i, j))$ for $i \in [n_r], j \in [n_c]$, set $n_r = 10, n_{r,0} = 4, n_c = 8, n_{c,0} = 3, \rho = 10$ and P as P_a . Panel (f) of Figure 10 shows an adjacency matrix A generated under BiMMDF for this set-up.

Model set-up 7: When $A(i, j) \sim \text{Logistic}(\Omega(i, j), \beta)$ for $i \in [n_r], j \in [n_c]$, set $n_r = 10, n_{r,0} = 4, n_c = 8, n_{c,0} = 3, \beta = 1, \rho = 40$ and P as P_b . Panel (g) of Figure 10 shows an adjacency matrix A generated under BiMMDF for this set-up.

Model set-up 8: For bipartite signed network when $\mathbb{P}(A(i, j) = 1) = \frac{1+\Omega(i, j)}{2}$ and $\mathbb{P}(A(i, j) = -1) = \frac{1-\Omega(i, j)}{2}$ for $i \in [n_r], j \in [n_c]$, set $n_r = 32, n_{r,0} = 14, n_c = 28, n_{c,0} = 12, \rho = 0.9$ and P as P_b . Panel (h) of Figure 10 shows an adjacency matrix A generated under BiMMDF for this set-up.

5.2 Real-world directed weighted networks

Table 3: Basic information and summarized statistics of directed weighted networks studied in this paper.

	Node meaning	Edge meaning	True memberships	n	K	$\max_{i,j} A(i, j)$	$\min_{i,j} A(i, j)$	#Edges	%Positive edges
Crisis in a Cloister	Monk	Ratings	Unknown	18	Unknown	1	-1	189	53.97%
Highschool	Boy	Friendship	Unknown	70	Unknown	2	0	366	100%
Facebook-like Social Network	User	Messages	Unknown	1302	Unknown	98	0	19044	100%

Table 4: η_r, η_c , and Hamm_{r_c} for real-world directed weighted networks used in this paper.

data	η_r	η_c	Hamm_{r_c}
Crisis in a Cloister	0.4444	0.2778	0.4203
Highschool	0.4571	0.3857	0.1340
Facebook-like Social Network	0.4777	0.5983	0.3084

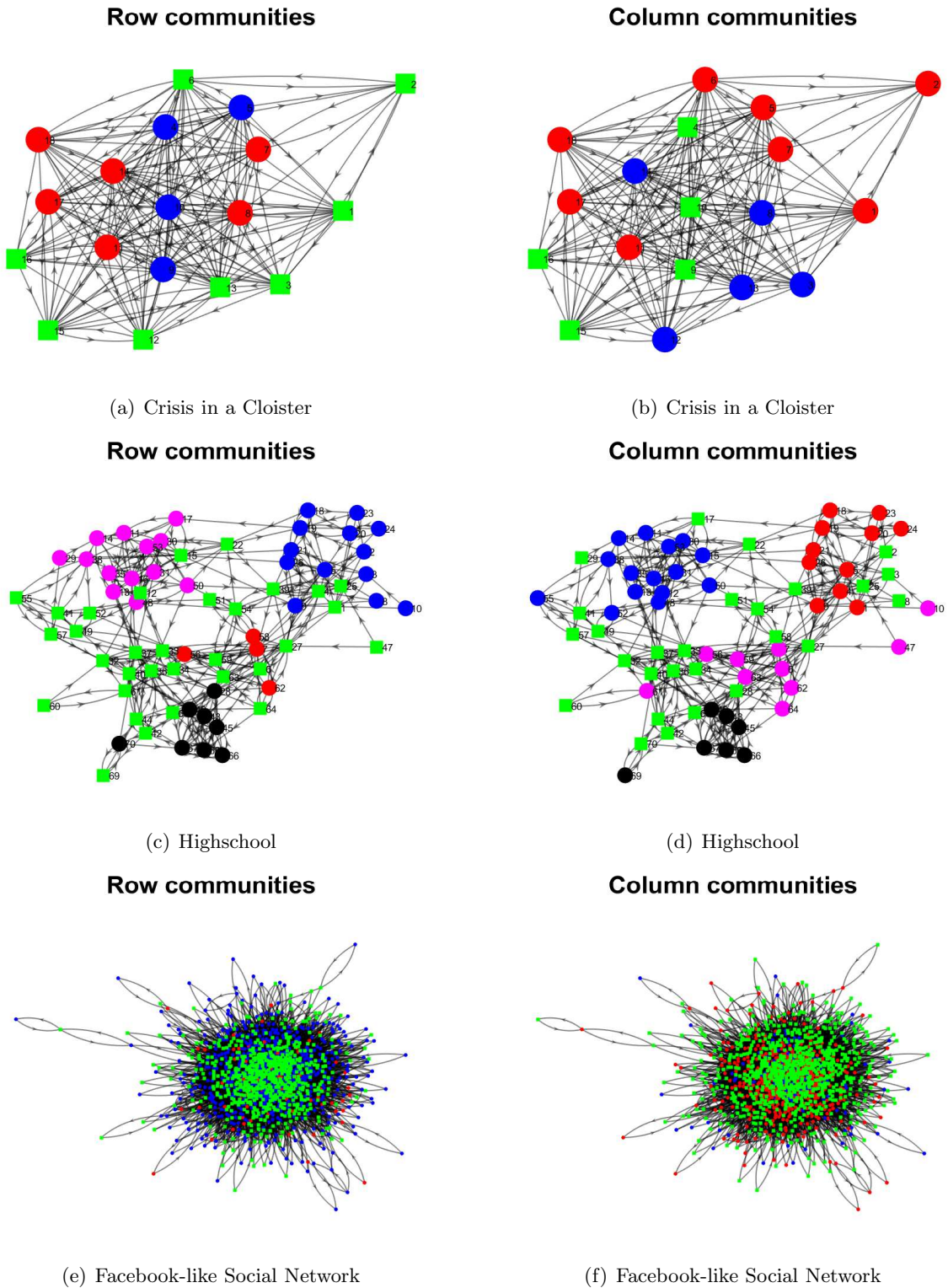


Figure 12: Row and column communities were detected by DiSP for real-world directed weighted networks used in this paper. Colors indicate communities and green square indicate highly mixed nodes, where the row and column communities are obtained by \hat{C}_r and \hat{C}_c , respectively. For visualization, we do not show edge weights here.

For real-world directed weighted networks used in this paper, row nodes are the same as column nodes, so $n_r = n_c = n$. Let $\hat{\mathcal{C}}_r$ be a vector whose i -th element is $\hat{\mathcal{C}}_r(i) = \operatorname{argmax}_{k \in [K]} \hat{\Pi}_r(i, k)$ for $i \in [n]$, and we call $\hat{\mathcal{C}}_r(i)$ the home base row community of node i . Define $\hat{\mathcal{C}}_c$ by letting $\hat{\mathcal{C}}_c(i) = \operatorname{argmax}_{k \in [K]} \hat{\Pi}_c(i, k)$ for $i \in [n]$. For node i , we call it highly mixed row node if $\max_{k \in [K]} \hat{\Pi}_r(i, k) \leq 0.8$. Let $\eta_r = \frac{|\{i: \max_{k \in [K]} \hat{\Pi}_r(i, k) \leq 0.8\}|}{n}$ be the proportion of highly mixed row nodes. Let η_c be the proportion of highly mixed column nodes and define it similar to η_r . Since $\mathcal{V}_r = \mathcal{V}_c$, to measure the asymmetric structure between row communities and column communities, we define a measurement Hamm_{rc} as $\text{Hamm}_{rc} = \frac{\min_{\mathcal{P} \in \mathcal{S}} \|\hat{\Pi}_r \mathcal{P} - \hat{\Pi}_c\|_1}{n}$, where large Hamm_{rc} suggests heavy asymmetric between row and column communities, vice versa. Note that for un-directed networks, Hamm_{rc} is 0, so we see that Hamm_{rc} is a good way to discover asymmetries in directed weighted networks.

Table 3 presents basic information and summarized statistics of real-world directed weighted networks used in this article. Crisis in a Cloister can be downloaded from http://konect.cc/networks/moreno_s (see also Kunegis (2013)), Highschool can be downloaded from http://konect.cc/networks/moreno_highsch and Facebook-like Social Network can be downloaded from https://toreopsahl.com/datasets/#online_soc. Note that for Facebook-like Social Network, the original data has 1899 nodes, where some nodes do not connect with any other nodes. Since we are only interested in the giant connected component of a network, after removing isolated nodes from both row and column sides, Facebook-like Social Network has 1302 nodes. To estimate K for these networks, we plot the top 10 singular values of A in Figure 11. For Crisis in a Cloister and Facebook-like Social network, the eigengap suggests $K = 2$, where Rohe et al. (2016) also uses eigengap to estimate K for real-world networks with unknown K . For Highschool, the eigengap suggests $K = 4$.

After having A and K , we apply DiSP to A , and report η_r, η_c and Hamm_{rc} in Table 4. The results show that Hamm_{rc} is large for these three datasets, and this indicates that the asymmetries between row and column communities for these datasets are heavy. Meanwhile, large η_r and η_c indicate that there exist large proportions of highly mixed nodes in both row and column communities for these networks. For better visibility of asymmetric structure for nodes, Figure 12 depicts row and column clusters returned by DiSP.

6. Conclusion and future work

In this paper, we propose a novel model, named the Bipartite Mixed Membership Distribution-Free (BiMMDF) model, to model the general bipartite weighted networks in which nodes can belong to multiple communities and all entries of adjacency matrices can be any finite real numbers. To the best of our knowledge, this is the first model to generate overlapping bipartite weighted networks. BiMMDF has no constraint on distributions of the adjacency matrix but only requires that the expectation adjacency matrix has a block structure that is directly related to node memberships for a bipartite weighted network. In particular, BiMMDF can model overlapping bipartite signed networks by choosing a carefully designed discrete distribution. An efficient spectral algorithm is used to fit BiMMDF. This algorithm can exactly return node memberships when using the expectation adjacency matrix Ω to replace the adjacency matrix A as input, and this guarantees BiMMDF's identifiability in turn. By considering the sparsity parameter ρ and distribution variance parameter γ , we build a general theoretical guarantee on estimation consistency for the algorithm under mild conditions under BiMMDF for any distribution. For a specific distribution, we can obtain respective theoretical upper bounds of error rates from the general theoretical results immediately as long as we have computed the distribution's variance parameter γ . The influence of ρ on the algorithm's performance, the range of ρ , and the upper bound of γ under different distributions are carefully analyzed based on our theoretical results in Examples 1-8. We also obtain the separation conditions of a standard bipartite weighted network for different distributions in Equation (2), where the algorithm's error rates are small with high probability as long as Equation (2) holds even when the network size is fixed. The separation conditions are carefully analyzed for different distributions in Examples 1-8, and we find that different distributions have different separation conditions. The

influence of ρ on the algorithm’s performance and the behavior difference phenomenon on separation conditions of different distributions are verified by substantial computer-generated bipartite weighted networks under BiMMDF. We also apply the algorithm to estimate node memberships for some real-world directed weighted networks with encouraging results. Our model BiMMDF is useful to model overlapping bipartite weighted networks with true node memberships under different distributions, and the algorithm DiSP used to fit BiMMDF can efficiently estimate node memberships for both computer-generated and real-world overlapping bipartite weighted networks. We expect that our BiMMDF model will have wide applications in complex networks to study the properties of bipartite weighted networks generated from any distribution, just as the mixed membership stochastic blockmodels has been widely studied in recent years.

One limitation of the algorithm used in this paper is, the number of communities K should be known in advance. Though we estimate K by eigengap like Rohe et al. (2016), rigorous methods should be developed to estimate K for bipartite weighted networks generated under BiMMDF under different distributions. Meanwhile, more than our BiMMDF, estimating K for all models listed in Table 2 is an open problem. Developing methods to estimate K for models in Table 2 is a challenging, interesting, and prospective topic. There are many ways to extend our work. First, in this paper, we use a spectral algorithm to fit BiMMDF because this spectral algorithm works for any distribution. It is possible to design new algorithms based on the ideas of nonnegative matrix factorization or likelihood maximization or tensor methods mentioned in Mao et al. (2020) to estimate node memberships for bipartite weighted networks generated under BiMMDF for a specific distribution. Second, like Rohe et al. (2011); Qin and Rohe (2013); Joseph and Yu (2016); Rohe et al. (2016), it is possible to design spectral algorithms based on applications of modified Laplacian matrix or regularized Laplacian matrix to fit BiMMDF. Third, it is also important to extend the idea developed in this paper to dynamic bipartite weighted networks and networks with covariates. Fourth, network mining task like link-prediction is an attractive topic for bipartite weighted networks generated under BiMMDF. There are many other ways to extend our work because BiMMDF is a generative model like SBM and MMSB. These ideas can also be applied to models in Table 2 for weighted networks. We leave studies of these interesting topics for our future work.

Acknowledgements

This research was funded by the High-level personal project of Jiangsu Province NO.JSSCBS20211218.

References

- Emmanuel Abbe. Community detection and stochastic block models: recent developments. *The Journal of Machine Learning Research*, 18(1):6446–6531, 2017.
- Emmanuel Abbe and Colin Sandon. Community detection in general stochastic block models: Fundamental limits and efficient algorithms for recovery. In *2015 IEEE 56th Annual Symposium on Foundations of Computer Science*, pages 670–688. IEEE, 2015.
- Emmanuel Abbe, Afonso S Bandeira, and Georgina Hall. Exact recovery in the stochastic block model. *IEEE Transactions on information theory*, 62(1):471–487, 2015.
- Kwangjun Ahn, Kangwook Lee, and Changho Suh. Hypergraph spectral clustering in the weighted stochastic block model. *IEEE Journal of Selected Topics in Signal Processing*, 12(5):959–974, 2018.
- Christopher Aicher, Abigail Z. Jacobs, and Aaron Clauset. Learning latent block structure in weighted networks. *Journal of Complex Networks*, 3(2):221–248, 2015.

- Edoardo M. Airoldi, David M. Blei, Stephen E. Fienberg, and Eric P. Xing. Mixed membership stochastic blockmodels. *Journal of Machine Learning Research*, 9:1981–2014, 2008.
- Edoardo M. Airoldi, Xiaopei Wang, and Xiaodong Lin. Multi-way blockmodels for analyzing coordinated high-dimensional responses. *The Annals of Applied Statistics*, 7(4):2431–2457, 2013.
- Animashree Anandkumar, Rong Ge, Daniel Hsu, and Sham Kakade. A tensor spectral approach to learning mixed membership community models. In *Conference on Learning Theory*, pages 867–881. PMLR, 2013.
- Brian Ball, Brian Karrer, and Mark EJ Newman. Efficient and principled method for detecting communities in networks. *Physical Review E*, 84(3):036103, 2011.
- Albert-Laszlo Barabasi and Zoltan N Oltvai. Network biology: understanding the cell’s functional organization. *Nature reviews genetics*, 5(2):101–113, 2004.
- Alain Barrat, Marc Barthélemy, Romualdo Pastor-Satorras, and Alessandro Vespignani. The architecture of complex weighted networks. *Proceedings of the National Academy of Sciences of the United States of America*, 101(11):3747–3752, 2004.
- Punam Bedi and Chhavi Sharma. Community detection in social networks. *Wiley Interdisciplinary Reviews: Data Mining and Knowledge Discovery*, 6(3):115–135, 2016.
- Peter J Bickel and Aiyu Chen. A nonparametric view of network models and newman–girvan and other modularities. *Proceedings of the National Academy of Sciences*, 106(50):21068–21073, 2009.
- Ronald L Breiger, Scott A Boorman, and Phipps Arabie. An algorithm for clustering relational data with applications to social network analysis and comparison with multidimensional scaling. *Journal of mathematical psychology*, 12(3):328–383, 1975.
- Yudong Chen, Xiaodong Li, and Jiaming Xu. Convexified modularity maximization for degree-corrected stochastic block models. *The Annals of Statistics*, 46(4):1573–1602, 2018.
- Yuxin Chen, Yuejie Chi, Jianqing Fan, Cong Ma, et al. Spectral methods for data science: A statistical perspective. *Foundations and Trends® in Machine Learning*, 14(5):566–806, 2021.
- James Samuel Coleman et al. Introduction to mathematical sociology. *Introduction to mathematical sociology.*, 1964.
- Adrien Dulac, Eric Gaussier, and Christine Largeron. Mixed-membership stochastic block models for weighted networks. In *Conference on Uncertainty in Artificial Intelligence*, pages 679–688. PMLR, 2020.
- Jennifer A. Dunne, Richard J. Williams, and Neo D. Martinez. Food-web structure and network theory: The role of connectance and size. *Proceedings of the National Academy of Sciences of the United States of America*, 99(20):12917, 2002.
- Santo Fortunato. Community detection in graphs. *Physics reports*, 486(3-5):75–174, 2010.
- Santo Fortunato and Darko Hric. Community detection in networks: A user guide. *Physics reports*, 659:1–44, 2016.
- Santo Fortunato and Mark EJ Newman. 20 years of network community detection. *Nature Physics*, 18(8):848–850, 2022.
- Nicolas Gillis and Stephen A. Vavasis. Semidefinite programming based preconditioning for more robust near-separable nonnegative matrix factorization. *SIAM Journal on Optimization*, 25(1): 677–698, 2015.

- Anna Goldenberg, Alice X Zheng, Stephen E Fienberg, Edoardo M Airoldi, et al. A survey of statistical network models. *Foundations and Trends® in Machine Learning*, 2(2):129–233, 2010.
- P.K. Gopalan and D.M. Blei. Efficient discovery of overlapping communities in massive networks. *Proceedings of the National Academy of Sciences of the United States of America*, 110(36):14534–14539, 2013.
- Roger Guimera and Luís A Nunes Amaral. Functional cartography of complex metabolic networks. *nature*, 433(7028):895–900, 2005.
- Bruce Hajek, Yihong Wu, and Jiaming Xu. Achieving exact cluster recovery threshold via semidefinite programming: Extensions. *IEEE Transactions on Information Theory*, 62(10):5918–5937, 2016.
- Paul W. Holland, Kathryn Blackmond Laskey, and Samuel Leinhardt. Stochastic blockmodels: First steps. *Social Networks*, 5(2):109–137, 1983.
- Muhammad Aqib Javed, Muhammad Shahzad Younis, Siddique Latif, Junaid Qadir, and Adeel Baig. Community detection in networks: A multidisciplinary review. *Journal of Network and Computer Applications*, 108:87–111, 2018.
- Pengsheng Ji and Jiashun Jin. Coauthorship and citation networks for statisticians. *The Annals of Applied Statistics*, 10(4):1779–1812, 2016.
- Pengsheng Ji, Jiashun Jin, Zheng Tracy Ke, and Wanshan Li. Co-citation and co-authorship networks of statisticians. *Journal of Business & Economic Statistics*, 40(2):469–485, 2022.
- Di Jin, Zhizhi Yu, Pengfei Jiao, Shirui Pan, Dongxiao He, Jia Wu, Philip Yu, and Weixiong Zhang. A survey of community detection approaches: From statistical modeling to deep learning. *IEEE Transactions on Knowledge and Data Engineering*, 2021.
- Jiashun Jin. Fast community detection by SCORE. *Annals of Statistics*, 43(1):57–89, 2015.
- Jiashun Jin, Zheng Tracy Ke, and Shengming Luo. Estimating network memberships by simplex vertex hunting. *arXiv preprint arXiv:1708.07852*, 2017.
- Antony Joseph and Bin Yu. Impact of regularization on spectral clustering. *The Annals of Statistics*, 44(4):1765–1791, 2016.
- Brian Karrer and M. E. J. Newman. Stochastic blockmodels and community structure in networks. *Physical Review E*, 83(1):16107, 2011.
- Emilie Kaufmann, Thomas Bonald, and Marc Lelarge. A spectral algorithm with additive clustering for the recovery of overlapping communities in networks. *Theoretical Computer Science*, 742:3–26, 2018.
- Jérôme Kunegis. Konect: the koblenz network collection. In *Proceedings of the 22nd international conference on world wide web*, pages 1343–1350, 2013.
- Pierre Latouche, Etienne Birmelé, and Christophe Ambroise. Overlapping stochastic block models with application to the french political blogosphere. *The Annals of Applied Statistics*, 5(1):309–336, 2011.
- Can M Le, Elizaveta Levina, and Roman Vershynin. Optimization via low-rank approximation for community detection in networks. *The Annals of Statistics*, 44(1):373–400, 2016.
- Jing Lei and Alessandro Rinaldo. Consistency of spectral clustering in stochastic block models. *Annals of Statistics*, 43(1):215–237, 2015.

- Elizabeth A Leicht and Mark EJ Newman. Community structure in directed networks. *Physical review letters*, 100(11):118703, 2008.
- Fragkiskos D Malliaros and Michalis Vazirgiannis. Clustering and community detection in directed networks: A survey. *Physics reports*, 533(4):95–142, 2013.
- Xueyu Mao, Purnamrita Sarkar, and Deepayan Chakrabarti. On mixed memberships and symmetric nonnegative matrix factorizations. *International Conference on Machine Learning*, pages 2324–2333, 2017.
- Xueyu Mao, Purnamrita Sarkar, and Deepayan Chakrabarti. Overlapping clustering models, and one (class) svm to bind them all. In *Advances in Neural Information Processing Systems*, volume 31, pages 2126–2136, 2018.
- Xueyu Mao, Purnamrita Sarkar, and Deepayan Chakrabarti. Estimating mixed memberships with sharp eigenvector deviations. *Journal of the American Statistical Association*, pages 1–13, 2020.
- M. E. J. Newman. Coauthorship networks and patterns of scientific collaboration. *Proceedings of the National Academy of Sciences*, 101(suppl 1):5200–5205, 2004a.
- Mark EJ Newman. Assortative mixing in networks. *Physical review letters*, 89(20):208701, 2002.
- Mark EJ Newman. The structure and function of complex networks. *SIAM review*, 45(2):167–256, 2003.
- Mark EJ Newman. Analysis of weighted networks. *Physical review E*, 70(5):056131, 2004b.
- Tin Lok James Ng and Thomas Brendan Murphy. Weighted stochastic block model. *Statistical Methods & Applications*, 30(5):1365–1398, 2021.
- Richard A Notebaart, Frank HJ van Enckevort, Christof Francke, Roland J Siezen, and Bas Teusink. Accelerating the reconstruction of genome-scale metabolic networks. *BMC Bioinformatics*, 7:296, 2006.
- Tore Opsahl and Pietro Panzarasa. Clustering in weighted networks. *Social networks*, 31(2):155–163, 2009.
- Gergely Palla, Albert-László Barabási, and Tamás Vicsek. Quantifying social group evolution. *Nature*, 446(7136):664–667, 2007.
- John Palowitch, Shankar Bhamidi, and Andrew B Nobel. Significance-based community detection in weighted networks. *J. Mach. Learn. Res.*, 18:188–1, 2017.
- Symeon Papadopoulos, Yiannis Kompatsiaris, Athena Vakali, and Ploutarchos Spyridonos. Community detection in social media. *Data mining and knowledge discovery*, 24(3):515–554, 2012.
- Clara Pizzuti. Ga-net: A genetic algorithm for community detection in social networks. In *International Conference on Parallel Problem Solving from Nature*, pages 1081–1090. Springer, 2008.
- Ioannis Psorakis, Stephen Roberts, Mark Ebdon, and Ben Sheldon. Overlapping community detection using bayesian non-negative matrix factorization. *Physical Review E*, 83(6):066114, 2011.
- Tai Qin and Karl Rohe. Regularized spectral clustering under the degree-corrected stochastic blockmodel. *Advances in Neural Information Processing Systems 26*, pages 3120–3128, 2013.
- Huan Qing. Distribution-free model for community detection. *arXiv preprint arXiv:2111.07495v3*, 2021.

- Huan Qing. A useful criterion on studying consistent estimation in community detection. *Entropy*, 24(8):1098, 2022a.
- Huan Qing. Degree-corrected distribution-free model for community detection in weighted networks. *Scientific Reports*, 12(1):1–19, 2022b.
- Huan Qing. Mixed membership distribution-free model. *arXiv preprint arXiv:2112.04389*, 2022c.
- Huan Qing and Jingli Wang. Directed mixed membership stochastic blockmodel. *arXiv preprint arXiv:2101.02307v3*, 2021.
- Huan Qing and Jingli Wang. Community detection for directed weighted networks. *arXiv preprint arXiv:2109.10319v3*, 2022.
- Karl Rohe, Sourav Chatterjee, and Bin Yu. Spectral clustering and the high-dimensional stochastic blockmodel. *The Annals of Statistics*, 39(4):1878–1915, 2011.
- Karl Rohe, Tai Qin, and Bin Yu. Co-clustering directed graphs to discover asymmetries and directional communities. *Proceedings of the National Academy of Sciences of the United States of America*, 113(45):12679–12684, 2016.
- Mikhail Rubinov and Olaf Sporns. Complex network measures of brain connectivity: uses and interpretations. *Neuroimage*, 52(3):1059–1069, 2010.
- Gang Su, Allan Kuchinsky, John H Morris, David J States, and Fan Meng. Glay: community structure analysis of biological networks. *Bioinformatics*, 26(24):3135–3137, 2010.
- Fei Wang, Tao Li, Xin Wang, Shenghuo Zhu, and Chris Ding. Community discovery using nonnegative matrix factorization. *Data Mining and Knowledge Discovery*, 22(3):493–521, 2011.
- Xiao Wang, Xiaochun Cao, Di Jin, Yixin Cao, and Dongxiao He. The (un) supervised nmf methods for discovering overlapping communities as well as hubs and outliers in networks. *Physica A: Statistical Mechanics and its Applications*, 446:22–34, 2016.
- Zhe Wang, Yingbin Liang, and Pengsheng Ji. Spectral algorithms for community detection in directed networks. *Journal of Machine Learning Research*, 21(153):1–45, 2020.
- Jierui Xie, Stephen Kelley, and Boleslaw K Szymanski. Overlapping community detection in networks: The state-of-the-art and comparative study. *Acm computing surveys (csur)*, 45(4):1–35, 2013.
- Min Xu, Varun Jog, and Po-Ling Loh. Optimal rates for community estimation in the weighted stochastic block model. *Annals of Statistics*, 48(1):183–204, 2020.
- Yuan Zhang, Elizaveta Levina, and Ji Zhu. Detecting overlapping communities in networks using spectral methods. *SIAM Journal on Mathematics of Data Science*, 2(2):265–283, 2020.
- Yunpeng Zhao, Elizaveta Levina, and Ji Zhu. Consistency of community detection in networks under degree-corrected stochastic block models. *The Annals of Statistics*, 40(4):2266–2292, 2012.
- Zhixin Zhou and Arash A.Amini. Analysis of spectral clustering algorithms for community detection: the general bipartite setting. *Journal of Machine Learning Research*, 20(47):1–47, 2019.

Appendix A. Proof of theoretical results for DiSP

A.1 Proof of Theorem 1

Proof Let $H_{\hat{U}} = \hat{U}'U$, and $H_{\hat{U}} = U_{H_{\hat{U}}} \Sigma_{H_{\hat{U}}} V_{H_{\hat{U}}}'$ be the top- K SVD of $H_{\hat{U}}$. Define $\text{sgn}(H_{\hat{U}}) = U_{H_{\hat{U}}} V_{H_{\hat{U}}}'$. Let $H_{\hat{V}} = \hat{V}'V$, and $H_{\hat{V}} = U_{H_{\hat{V}}} \Sigma_{H_{\hat{V}}} V_{H_{\hat{V}}}'$ be the top- K SVD of $H_{\hat{V}}$. Define $\text{sgn}(H_{\hat{V}}) = U_{H_{\hat{V}}} V_{H_{\hat{V}}}'$. Based on our model BiMMDF and Assumptions 1-3 and Condition 1, we have below results:

- $\mathbb{E}[A(i, j) - \Omega(i, j)] = 0$ under BiMMDF.
- $\mathbb{E}[(A(i, j) - \Omega(i, j))^2] \leq \rho\gamma$ by Assumption 2.
- Let $\mu = \max(\frac{n_r \|U\|_{2 \rightarrow \infty}^2}{K}, \frac{n_c \|V\|_{2 \rightarrow \infty}^2}{K})$ be the incoherence parameter defined in Definition 3.1. Chen et al. (2021). By Lemma 8 Qing and Wang (2021) and Condition 1, we have $\mu = O(1)$.
- Let $c_b = \frac{\tau}{\sqrt{\rho\gamma \min(n_r, n_c) / (\mu \log(n_r + n_c))}}$. By Condition 1, we have $\min(n_r, n_c) = O(\max(n_r, n_c))$. By the fact that $\mu = O(1)$ given in the last bullet and Assumptions 1 and 3, we have $c_b \leq O(1)$.
- By $\kappa(P) = O(1)$ in Condition 1 and Lemma 10 Qing and Wang (2021), we have $\kappa(\Omega) = O(1)$.

The first four bullets suggest that the settings and assumptions of Theorem 4.4 Chen et al. (2021) are satisfied, so by Theorem 4.4. Chen et al. (2021), with probability at least $1 - O(\frac{1}{(n_r + n_c)^5})$, we have

$$\max(\|\hat{U} \text{sgn}(H_{\hat{U}}) - U\|_{2 \rightarrow \infty}, \|\hat{V} \text{sgn}(H_{\hat{V}}) - V\|_{2 \rightarrow \infty}) \leq C \frac{\sqrt{\rho\gamma K \log(n_r + n_c)}}{\sigma_K(\Omega)},$$

provided that $\sigma_K(\Omega) \gg \sqrt{\rho\gamma(n_r + n_c) \log(n_r + n_c)}$.

For convenience, let $\varpi = \max(\|\hat{U}\hat{U}' - UU'\|_{2 \rightarrow \infty}, \|\hat{V}\hat{V}' - VV'\|_{2 \rightarrow \infty})$ be the row-wise singular vector error. Since $\|\hat{U}\hat{U}' - UU'\|_{2 \rightarrow \infty} \leq 2\|U - \hat{U} \text{sgn}(H_{\hat{U}})\|_{2 \rightarrow \infty}$ and $\|\hat{V}\hat{V}' - VV'\|_{2 \rightarrow \infty} \leq 2\|V - \hat{V} \text{sgn}(H_{\hat{V}})\|_{2 \rightarrow \infty}$, we have

$$\varpi \leq C \frac{\sqrt{\rho\gamma K \log(n_r + n_c)}}{\sigma_K(\Omega)}.$$

Lemma 10 Qing and Wang (2021) gives $\sigma_K(\Omega) \geq \rho\sigma_K(P)\sigma_K(\Pi_r)\sigma_K(\Pi_c)$, so we have

$$\varpi \leq C \frac{\sqrt{\gamma K \log(n_r + n_c)}}{\sigma_K(P)\sigma_K(\Pi_r)\sigma_K(\Pi_c)\sqrt{\rho}}.$$

By Assumption 3, we have $\sigma_K(\Pi_r) = O(\sqrt{\frac{n_r}{K}})$ and $\sigma_K(\Pi_c) = O(\sqrt{\frac{n_c}{K}})$, which gives

$$\varpi \leq C \frac{K^{1.5} \sqrt{\gamma \log(n_r + n_c)}}{\sigma_K(P) \sqrt{\rho n_r n_c}}. \quad (11)$$

By Theorem 2 Qing and Wang (2021) where the proof is distribution-free, there exist two permutation matrices $\mathcal{P}_r, \mathcal{P}_c \in \mathbb{R}^{K \times K}$ such that for $i \in [n_r], j \in [n_c]$,

$$\|e'_i(\hat{\Pi}_r - \Pi_r \mathcal{P}_r)\|_1 = O(\varpi \kappa(\Pi_r' \Pi_r) K \sqrt{\lambda_1(\Pi_r' \Pi_r)}), \|e'_j(\hat{\Pi}_c - \Pi_c \mathcal{P}_c)\|_1 = O(\varpi \kappa(\Pi_c' \Pi_c) K \sqrt{\lambda_1(\Pi_c' \Pi_c)}). \quad (12)$$

By Assumption 3 and Equation (11), we have

$$\|e'_i(\hat{\Pi}_r - \Pi_r \mathcal{P}_r)\|_1 = O\left(\frac{K^2 \sqrt{\gamma \log(n_r + n_c)}}{\sigma_K(P) \sqrt{\rho n_c}}\right), \|e'_j(\hat{\Pi}_c - \Pi_c \mathcal{P}_c)\|_1 = O\left(\frac{K^2 \sqrt{\gamma \log(n_r + n_c)}}{\sigma_K(P) \sqrt{\rho n_r}}\right).$$

Remark 6 Without Assumption 3, the error bounds of DiSP are always the same as that of Equation (12). In this paper, we consider Assumption 3 mainly for theoretical convenience. ■

A.2 Proof of Corollary 1

Proof For $BiMMDF(n, 2, \Pi_r, \Pi_c, \alpha_{in}, \alpha_{out}, \mathcal{F})$, since $K = 2$, by basic algebra, we have $\sigma_K(\rho P) = \sigma_2(\rho P) = \||p_{in}| - |p_{out}|\| = \rho\sigma_2(P)$. Recall that we let $\max_{k,l \in [K]} |P(k,l)| = 1$ in Definition 1, we have $\max_{k,l \in [K]} |\rho P(k,l)| = \rho = \max(|p_{in}|, |p_{out}|)$, which gives that $\frac{\||p_{in}| - |p_{out}|\|}{\sqrt{\max(|p_{in}|, |p_{out}|)}} = \sqrt{\rho}\sigma_K(P)$ should shrink slower than $\sqrt{\frac{\gamma \log(n)}{n}}$ for small error rates with high probability by Theorem 1. Since $\frac{\||p_{in}| - |p_{out}|\|}{\sqrt{\max(|p_{in}|, |p_{out}|)}} = \frac{\||\alpha_{in}| - |\alpha_{out}|\|}{\sqrt{\max(|\alpha_{in}|, |\alpha_{out}|)}} \sqrt{\frac{\log(n)}{n}}$, $\frac{\||\alpha_{in}| - |\alpha_{out}|\|}{\sqrt{\max(|\alpha_{in}|, |\alpha_{out}|)}}$ should shrink slower than $\sqrt{\gamma}$ for small error rates with high probability, i.e.,

$$\frac{\||\alpha_{in}| - |\alpha_{out}|\|}{\sqrt{\max(|\alpha_{in}|, |\alpha_{out}|)}} \gg \sqrt{\gamma}. \quad (13)$$

Meanwhile, since $\rho = \max(|p_{in}|, |p_{out}|) = \frac{\log(n)}{n} \max(|\alpha_{in}|, |\alpha_{out}|)$ under $BiMMDF(n, 2, \Pi_r, \Pi_c, \alpha_{in}, \alpha_{out}, \mathcal{F})$, we have $\frac{\log(n)}{n} \max(|\alpha_{in}|, |\alpha_{out}|) \gamma n \geq \tau^2 \log(2n)$ by Assumption 1, which gives

$$\gamma \max(|\alpha_{in}|, |\alpha_{out}|) \geq \tau^2 \frac{\log(2n)}{\log(n)}. \quad (14)$$

Now, when Equation (14) holds, Equation (13) can be released as

$$\||\alpha_{in}| - |\alpha_{out}|\| \gg \tau \sqrt{\frac{\log(2n)}{\log(n)}}. \quad (15)$$

Since $\frac{\log(2n)}{\log(n)} = \frac{\log(2)}{\log(n)} + 1 = 1 + o(1)$ when n is not too small, Equations (14) and (15) can be released as

$$\gamma \max(|\alpha_{in}|, |\alpha_{out}|) \geq \tau^2 + o(1) \text{ and } \||\alpha_{in}| - |\alpha_{out}|\| \gg \tau. \quad (16)$$

Next we show that the lower bound requirement of $\sigma_K(\Omega)$ in Theorem 1 and $\kappa(P) = O(1)$ in Condition 1 hold naturally as long as Equation (16) holds. By Lemma Qing and Wang (2021), we know that $\sigma_2(\Omega) \geq \rho\sigma_2(P)\sigma_2(\Pi_r)\sigma_2(\Pi_c)$ holds under $BiMMDF(n, 2, \Pi_r, \Pi_c, \alpha_{in}, \alpha_{out}, \mathcal{F})$ without other assumptions. Therefore, to guarantee that the condition $\sigma_2(\Omega) \gg \sqrt{\rho\gamma n \log(2n)}$ in Theorem 1 always holds when $n_r = n_c = n$ and $K = 2$ under $BiMMDF(n, 2, \Pi_r, \Pi_c, \alpha_{in}, \alpha_{out}, \mathcal{F})$, we need $\rho\sigma_2(P)\sigma_2(\Pi_r)\sigma_2(\Pi_c) \gg \sqrt{\rho\gamma n \log(2n)} = \sqrt{\rho\gamma n (\log(2) + \log(n))} = O(\sqrt{\rho\gamma n \log(n)})$, i.e.,

$$\sigma_2(P) \gg \sqrt{\frac{\gamma n \log(n)}{\rho \lambda_2(\Pi_r' \Pi_r) \lambda_2(\Pi_c' \Pi_c)}}. \quad (17)$$

Since $\lambda_2(\Pi_r' \Pi_r) = O(\frac{n}{2}) = O(n)$, $\lambda_2(\Pi_c' \Pi_c) = O(\frac{n}{2}) = O(n)$ under $BiMMDF(n, 2, \Pi_r, \Pi_c, \alpha_{in}, \alpha_{out}, \mathcal{F})$, Equation (17) gives that $\sigma_2(P)$ should shrink slower than $\sqrt{\frac{\gamma \log(n)}{\rho n}}$, which matches with the consistency requirement on $\sigma_2(P)$ obtained from Theorem 1 under $BiMMDF(n, 2, \Pi_r, \Pi_c, \alpha_{in}, \alpha_{out}, \mathcal{F})$. Therefore, under $BiMMDF(n, 2, \Pi_r, \Pi_c, \alpha_{in}, \alpha_{out}, \mathcal{F})$, the lower bound requirement on $\sigma_K(\Omega)$ in Theorem 1 holds naturally as long as Equation (16) holds. Finally, since $\kappa(P) = \kappa(\rho P) = \frac{\||\alpha_{in}| + |\alpha_{out}|\|}{\||\alpha_{in}| - |\alpha_{out}|\|}$, we see that $\kappa(P) = O(1)$ in Condition 1 holds immediately when Equation (16) holds. ■